© 2017. Published by The Company of Biologists Ltd | Journal of Cell Science (2017) 130, 563-576 doi:10.1242/jcs.197004

RESEARCH ARTICLE

Regulation of ciliary retrograde protein trafficking by the Joubert syndrome proteins ARL13B and INPP5E

Shohei Nozaki[1,*], Yohei Katoh[1,*], Masaya Terada[1], Saki Michisaka[1], Teruki Funabashi[1], Senye Takahashi[1], Kenji Kontani[2] and Kazuhisa Nakayama[1,‡]

ABSTRACT

ARL13B (a small GTPase) and INPP5E (a phosphoinositide 5-phosphatase) are ciliary proteins encoded by causative genes of Joubert syndrome. We here showed, by taking advantage of a visible immunoprecipitation assay, that ARL13B interacts with the IFT46–IFT56 (IFT56 is also known as TTC26) dimer of the intraflagellar transport (IFT)-B complex, which mediates anterograde ciliary protein trafficking. However, the ciliary localization of ARL13B was found to be independent of its interaction with IFT-B, but dependent on the ciliary-targeting sequence RVEP in its C-terminal region. *ARL13B*-knockout cells had shorter cilia than control cells and exhibited aberrant localization of ciliary proteins, including INPP5E. In particular, in *ARL13B*-knockout cells, the IFT-A and IFT-B complexes accumulated at ciliary tips, and GPR161 (a negative regulator of Hedgehog signaling) could not exit cilia in response to stimulation with Smoothened agonist. This abnormal phenotype was rescued by the exogenous expression of wild-type ARL13B, as well as by its mutant defective in the interaction with IFT-B, but not by its mutants defective in INPP5E binding or in ciliary localization. Thus, ARL13B regulates IFT-A-mediated retrograde protein trafficking within cilia through its interaction with INPP5E.

KEY WORDS: ARL13B, Cilia, IFT-A complex, IFT-B complex, INPP5E, VIP assay

INTRODUCTION

The small GTPase family of ARF (ADP-ribosylation factor) and ARL (ARF-like), and that of RAB act as molecular switches by cycling between a GDP-bound inactive state and a GTP-bound active state to regulate a wide variety of membrane trafficking events. ARF and RAB GTPases also play important roles in protein trafficking to and within cilia (Li and Hu, 2011; Lim et al., 2011), and the specific GTPases involved include ARF4, ARL3, ARL6, ARL13B, RAB8A and RAB8B, RAB10, RAB11, RAB23 and RAB28.

Cilia are microtubule-based structures projecting from the plasma membrane of most cells in the human body and other ciliated organisms. Although the ciliary membrane is continuous with the plasma membrane, the composition of proteins and lipids within cilia and on ciliary membranes is completely different from that in the cytoplasm and on the plasma membrane due to the presence of the transition zone, which functions as a diffusion or permeability barrier located at the base of cilia (Sung and Leroux, 2013; Wei et al., 2015). Cilia play crucial roles in the perception of physiological stimuli and the transduction of developmental signals via a group of ciliary receptors and ion channels that process these extracellular inputs. Therefore, defects in the assembly or functions of cilia lead to genetic disorders, collectively called ciliopathies, which result in a wide range of symptoms, including retinal degeneration, polycystic kidney, and brain and skeletal malformations (Brown and Witman, 2014; Madhivanan and Aguilar, 2014; Schwartz et al., 2011). These disorders include Bardet–Biedl syndrome (BBS), Joubert syndrome (JBTS), Meckel syndrome (MKS), nephronophthisis and short-rib thoracic dysplasia (SRTD).

Bidirectional trafficking of proteins along axoneme microtubules within cilia is mediated by the intraflagellar transport (IFT) machinery, which comprises two large multi-protein complexes, namely, IFT-A (composed of six subunits, which are associated with TULP3) and IFT-B (16 subunits) (Katoh et al., 2016; Taschner et al., 2012; Wei et al., 2015). The anterograde trafficking of proteins from the base to the tip of cilia is mediated by the IFT-B complex, which works together with kinesin-2 motor proteins. In contrast, retrograde protein trafficking is mediated by the IFT-A complex, which works together with dynein-2. The lack of an IFT-A or IFT-B subunit often results in extremely short or no cilia (for example, see Huangfu et al., 2003; Jonassen et al., 2008; Liem et al., 2012), implying a defect in the trafficking of proteins essential for ciliary assembly. Furthermore, mutations in some of the IFT-A and IFT-B subunits are known to cause BBS and SRTD: IFT121 (*SRTD7*), IFT139 (*SRTD4*), IFT140 (*SRTD9*), and IFT144 (*SRTD5*) of the IFT-A complex; and IFT27 (*BBS19*), IFT52 (*SRTD16*), IFT80 (*SRTD2*), IFT172 (*BBS20* or *SRTD10*) of the IFT-B complex (Cortés et al., 2015; Geister and Camper, 2015).

Mutations in the *ARL13B* gene (also known as *JBTS8*) is one of the causative agents of JBTS (Cantagrel et al., 2008; Madhivanan and Aguilar, 2014; Romani et al., 2013), and has been used as a marker of cilia in a number of studies. Pioneering studies of Caspary, Anderson and colleagues have demonstrated that *ARL13B* mutant mice, named *hennin*, exhibit defects in axoneme organization and in Hedgehog (Hh) signaling (Caspary et al., 2007; Larkins et al., 2011). However, the roles of ARL13B are not fully understood from the viewpoint of ciliary protein trafficking. ARL13B has been shown to interact with and participate in the ciliary targeting of another JBTS protein INPP5E (the gene encoding this protein is also known as *JBTS1*) (Humbert et al., 2012), which is a phosphoinositide 5-phosphatase. Recently, ARL13B has been reported to serve as a guanine nucleotide exchange factor (GEF) for ARL3 (Gotthardt et al., 2015), which interacts with PDE6D (Linari et al., 1999; Van Valkenburgh et al., 2001), another JBTS protein (the gene encoding this protein is also known as *JBTS22*). PDE6D is known to bind to C-terminally

[1]Graduate School of Pharmaceutical Sciences, Kyoto University, Sakyo-ku, Kyoto 606-8501, Japan. [2]Department of Biochemistry, Meiji Pharmaceutical University, Kiyose, Tokyo 204-8588, Japan.
*These authors contributed equally to this work

‡Author for correspondence (kazunaka@pharm.kyoto-u.ac.jp)

K.N., 0000-0001-7701-7183

Received 30 August 2016; Accepted 29 November 2016

Journal of Cell Science (2017) 130, 563-576 doi:10.1242/jcs.197004

prenylated proteins, including INPP5E, and ARL3 stimulates release of PDE6D from prenylated proteins (Fansa et al., 2016; Ismail et al., 2011). On the other hand, Blacque and colleagues have revealed that the IFT-B complex interacts with ARL13B and proposed that IFT-B facilitates the ciliary localization of ARL13B (namely, ARL13B might be a cargo of the IFT machinery), although it was uncertain which subunit(s) of the IFT-B complex are responsible for its interaction with ARL13B (Cevik et al., 2013).

Recently, we developed a novel and flexible method for detecting protein–protein interactions, which we named the visible immunoprecipitation (VIP) assay (Katoh et al., 2015, 2016). By taking advantage of this flexible method, we previously determined the architecture of the IFT-B complex (Katoh et al., 2016), as well as those of the BBSome (a complex composed of eight subunits encoded by the causative genes of BBS) and exocyst complexes (Katoh et al., 2015). In the present study, we used the VIP assay to determine which subunit(s) of the IFT-B complex participate in its interaction with ARL13B, and found that the IFT46–IFT56 dimer (IFT56 is also known as TTC26) is responsible for the interaction of IFT-B with ARL13B [note that IFT56 is the most recently identified IFT-B component (Ishikawa et al., 2014), and IFT46 and IFT56 have been shown to form a heterodimer (Swiderski et al., 2014)]. We then constructed an ARL13B mutant that is defective in IFT-B binding, but found that this mutant retained the ability to localize throughout cilia, excluding the possibility that ARL13B is a cargo of the IFT machinery.

We then established *ARL13B*-knockout (KO) lines of human telomerase reverse transcriptase-immortalized retinal pigmented epithelial (hTERT-RPE1) cells using a modified CRISPR/Cas9 system, and showed that the phenotype of the *ARL13B*-KO cell lines resembles that of cells derived from *INPP5E*$^{-/-}$ mice. These findings provide new insights into not only the roles of ARL13B in ciliary protein trafficking but also the pathogenesis of ciliopathies.

RESULTS

ARL13B interacts with the IFT-B complex via the IFT46–IFT56 dimer

Although a previous study using proteomic analysis of affinity purified proteins and yeast two-hybrid analysis suggested that ARL13B interacts with some subunit(s) of the IFT-B complex (Cevik et al., 2013), it remained uncertain as to which subunit(s) directly interact with ARL13B. To unequivocally determine the subunits responsible for interaction of the IFT-B complex with ARL13B, we applied the VIP assay, which was established in our laboratory as a simple and versatile method to determine protein–protein interactions without performing SDS-PAGE and immunoblotting (Katoh et al., 2015, 2016). Using our VIP assay, we previously determined the overall architectures of the exocyst, BBSome and IFT-B complexes. The IFT-B complex is composed of 16 subunits that can be divided into the core and peripheral subcomplexes, composed of 10 subunits [IFT22, IFT25 (also known as HSPB11), IFT27, IFT46, IFT52, IFT56, IFT70 (also known as TTC30B), IFT74, IFT81 and IFT88] (Lucker et al., 2005; Taschner et al., 2014) and 6 subunits [IFT20, IFT38 (also known as CLUAP1), IFT54 (also known as TRAF3IP1), IFT57, IFT80 and IFT172], respectively, which are connected to each other by composite interactions involving IFT38, IFT52, IFT57 and IFT88 (Boldt et al., 2016; Katoh et al., 2016; Taschner et al., 2016) (also see Fig. 8).

First, we examined whether EGFP-fused ARL13B can interact with any one of the 16 IFT-B subunits when fused to TagRFP (tRFP) or mCherry (mChe), but failed to detect any clear interaction (data not shown). We then exploited one of the advantages of the flexible VIP assay system to detect the ARL13B–IFT-B interaction; previously, we successfully identified one-to-many and many-to-many subunit interactions in the exocyst and IFT-B complexes through the VIP assay (Katoh et al., 2015, 2016). When ARL13B–EGFP was co-expressed with all the core or peripheral subunits fused to tRFP or mChe in HEK293T cells, and lysates prepared from the transfected cells were processed for immunoprecipitation with glutathione *S*-transferase (GST)-fused anti-GFP nanobody (Nb) prebound to glutathione–Sepharose beads, red fluorescent signals were detected when the core, but not peripheral, subunits were co-expressed with ARL13B (Fig. 1A). These VIP data indicate that the IFT-B subunits responsible for ARL13B interaction are included in the core subcomplex.

We then applied a subtractive VIP assay to determine the IFT-B core subunits responsible for the interaction with ARL13B; in this assay, omitting one or more of the core subunits would be expected to abolish red signals if those core subunit(s) are crucial for the interaction between ARL13B and the core subcomplex. As shown in Fig. 1B, red fluorescent signals were extremely attenuated when IFT46 or IFT56 was omitted from the 10 core subunits fused to tRFP or mChe, suggesting that these two subunits participate in the interaction of the core subcomplex with ARL13B. To examine whether these two subunits are indeed responsible for the interaction with ARL13B, we then performed VIP assays to detect one-to-two protein interactions. As shown in Fig. 1C, red signals were detected only when ARL13B–tRFP was co-expressed with both EGFP–IFT46 and EGFP–IFT56. Co-immunoprecipitation of EGFP–IFT46 and EGFP–IFT56 with ARL13B–tRFP was confirmed by subjecting the immunoprecipitates to conventional immunoblotting analysis (Fig. 1D). We therefore concluded that ARL13B interacts with the IFT-B complex via the IFT46–IFT56 dimer (see Fig. 8).

A previous yeast two-hybrid study suggested that IFT46 and IFT74 interacted with ARL13B (Cevik et al., 2013). We therefore addressed whether IFT74 can also interact directly with ARL13B. In the model of the IFT-B architecture (Katoh et al., 2016; Taschner et al., 2014) (also see Fig. 8), IFT74, by forming a tight complex with IFT81 (Bhogaraju et al., 2013), interacts with the IFT46–IFT52 dimer, and IFT56 interacts with IFT46. As shown in Fig. 1E, ARL13B–EGFP could not co-precipitate mChe-tagged IFT74 alone (lane 1) or IFT74 plus IFT81 (lane 2). mChe-tagged IFT74 plus IFT81 was co-precipitated with ARL13B–EGFP in the presence of co-expressed IFT46, IFT52 and IFT56 (lane 5), but was not co-precipitated in the presence of IFT46 and IFT56 in the absence of IFT52 (lane 3). Thus, our data exclude the possibility that IFT74 has an ability to directly interact with ARL13B.

ARL13B interacts with the IFT46–IFT56 dimer via its C-terminal region, but not via the RVEP ciliary-targeting sequence

ARL13B not only has the GTP-binding domain that is typical of the ARF/ARL family of small GTPases, but also has an exceptionally long C-terminal region (see Fig. 2A). A previous study suggested that a mutation in the RVEP sequence in mammalian ARL13B (amino acid residues 358–361) abolishes the ciliary localization of ARL13B (Higginbotham et al., 2012) (also see Fig. 3H). In addition, the C-terminal RVVP sequence in *Caenorhabditis elegans* ARL-13 was suggested to determine its correct localization within cilia (Cevik et al., 2013). These sequences match the consensus ciliary-targeting motif (RVxP) found in several ciliary proteins (Geng et al., 2006). On the basis of our data showing that the IFT46–IFT56 dimer of the IFT-B complex, which mediates anterograde protein trafficking within the cilium, is responsible for the interaction of ARL13B with IFT-B, we hypothesized that the RVEP sequence could control the interaction. However, this was not

Journal of Cell Science (2017) 130, 563-576 doi:10.1242/jcs.197004

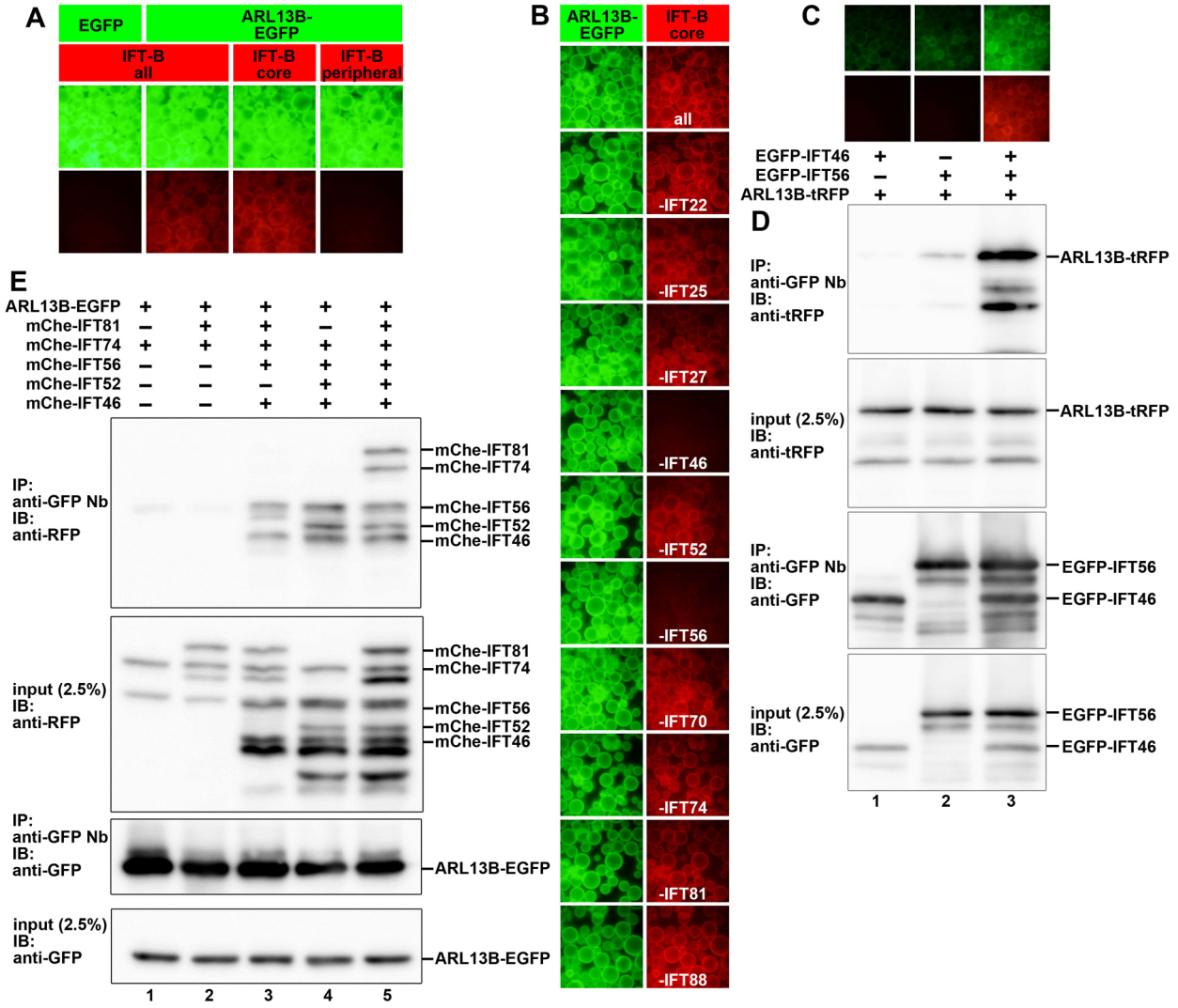

Fig. 1. Interaction of ARL13B with IFT46–IFT56 as demonstrated by the VIP assay. (A) Interaction of ARL13B with the IFT-B core subcomplex, as demonstrated by the VIP assay. HEK293T cells were co-transfected with an expression vector for EGFP or Arf13b–EGFP, together with expression vectors for all the subunits of the IFT-B complex, or the core or peripheral subcomplex, fused to tRFP or mChe. Lysates prepared from the transfected cells were processed for the VIP assay, as described in the Materials and Methods. (B) Subtractive VIP assays to determine the IFT-B core subunits involved in the interaction of IFT-B with ARL13B. HEK293T cells were co-transfected with expression vectors for ARL13B–EGFP and all but one (as indicated) of the core subunits fused to tRFP or mChe, and lysates prepared from the transfected cells were processed for the VIP assay. (C,D) Interaction of ARL13B with IFT46–IFT56. HEK293T cells were co-transfected with expression vectors for ARL13B–tRFP and either EGFP-fused IFT46 and/or IFT56, and lysates prepared from the transfected cells were processed for the VIP assay (C) or immunoprecipitation (IP) followed by immunoblotting (IB) analysis using an antibody against tRFP (D, top two panels) or GFP (D, bottom two panels). The labels under the images shown in C also apply to D. (E) IFT74 does not directly interact with ARL13B. HEK293T cells were co-transfected with expression vectors for ARL13B–EGFP and mChe-fused IFT46, IFT52, IFT56, IFT74 and/or IFT81 as indicated, and lysates prepared from the transfected cells were immunoprecipitated with GST-fused anti-GFP Nb and processed for immunoblotting analysis using an antibody against RFP (top two panels) or GFP (bottom two panels).

the case; an AAEA mutant, in which the RVEP sequence was changed to AAEA, retained the ability to interact with IFT46–IFT56 (Fig. 2B,C, lane 9).

We next constructed various ARL13B mutants and examined whether these mutants could interact with the IFT46–IFT56 dimer by using the VIP assay. These mutants included the following (see Fig. 2A): T35N, a GTPase-domain mutant expected to be locked in a GDP-bound inactive state; R79Q, another GTPase-domain mutant defective in GTP binding, which is found in Joubert syndrome patients (Cantagrel et al., 2008); ΔGD, which lacks the entire GTPase domain (residues 20–189); Arf6GD, in which the GTPase domain is replaced with the GTPase domain from ARF6; R200C, another mutant found in Joubert syndrome patients with an Arg-to-Cys replacement in the coiled-coil (CC) region (Cantagrel et al., 2008); ΔCC, which lacks the entire CC region (residues 190–244); AAEA (see above); and ΔPR, which lacks the C-terminal region containing a Pro-rich (PR) sequence (residues 362–428) located immediately after the RVEP sequence. Among these mutants, we found that ARL13B(ΔPR) completely lost the ability to interact with IFT46–IFT56 (Fig. 2B,C, lane 10; and summarized in Fig. 2A). The interaction of ARL13B(ΔGD) (lane 5), ARL13B(Arf6GD) (lane 6), or ARL13B(AAEA) (lane 9) with IFT46–IFT56 appeared relatively weak as compared with ARL13B(WT), but substantially stronger than with ARL13B (ΔPR), although we did not pursue these differences further in this study. Thus, the region C-terminal to the known ciliary-targeting

Journal of Cell Science (2017) 130, 563-576 doi:10.1242/jcs.197004

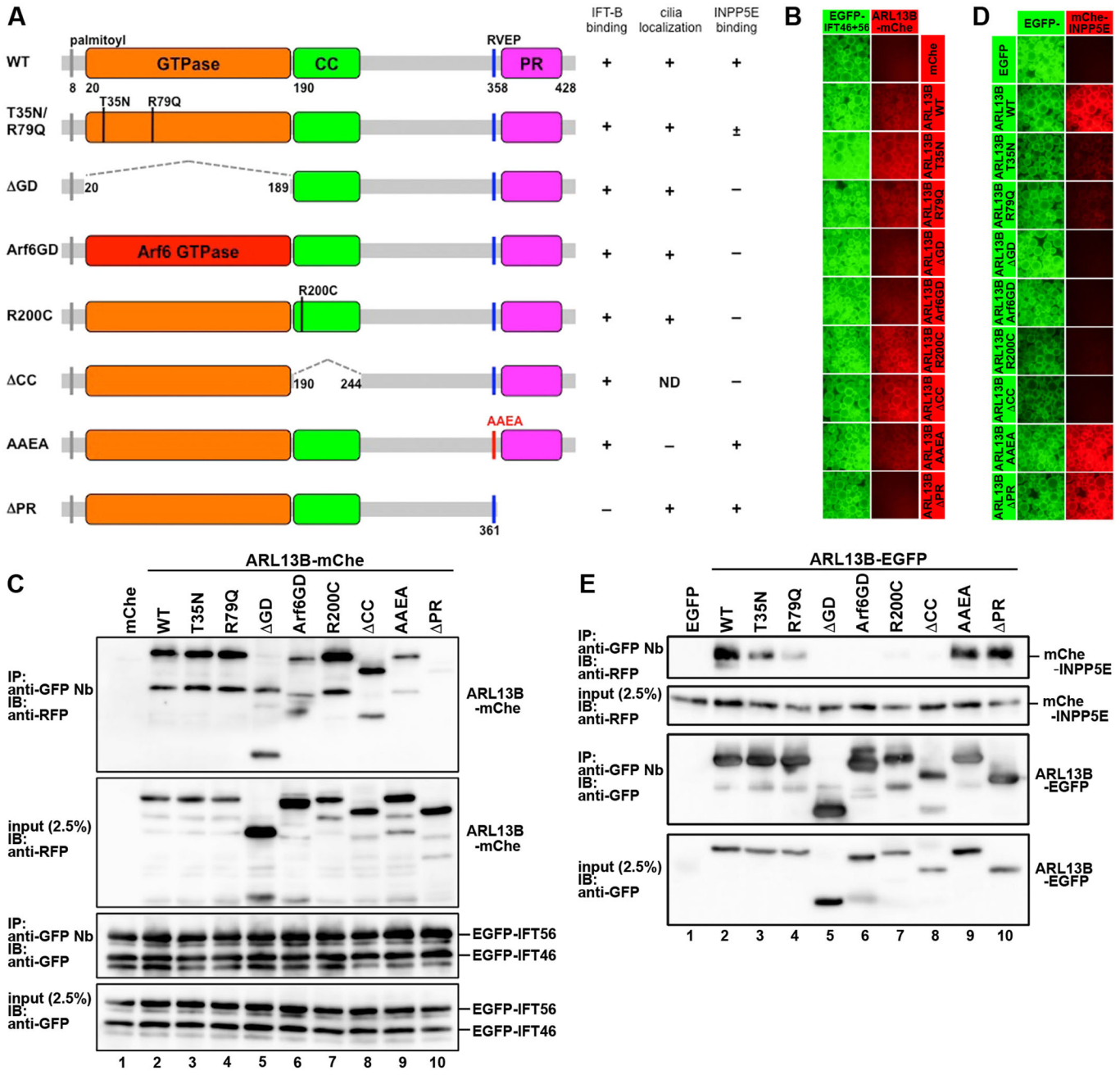

Fig. 2. Domains of ARL13B responsible for its interactions with IFT46–IFT56 and INPP5E. (A) Schematic representation of the ARL13B constructs used in this study. A summary of the results of the IFT-B binding, ciliary localization and INPP5E-binding experiments for each construct are shown on the right side of each construct. +, substantial binding or localization; ±, weak binding; –, no binding or localization; ND, not determined. (B,C) The proline-rich (PR) region of ARL13B is involved in its interaction with IFT46–IFT56. HEK293T cells were co-transfected with expression vectors for an ARL13B–mChe construct as indicated and for EGFP-fused IFT46 and IFT56, and lysates prepared from the transfected cells were processed for the VIP assay (B) or immunoprecipitation (IP) followed by immunoblotting (IB) analysis using an antibody against RFP (C, top two panels) or GFP (C, bottom two panels). (D,E) The GTPase domain and the CC region of ARL13B are involved in its interaction with INPP5E. HEK293T cells were co-transfected with expression vectors for an ARL13B–EGFP construct as indicated and for mChe-INPP5E, and lysates prepared from the transfected cells were processed for the VIP assay (D) or immunoprecipitation followed by immunoblotting analysis using an antibody against RFP (E, top two panels) or GFP (E, bottom two panels).

sequence is the major determinant of the interaction of ARL13B with the IFT-B complex.

Ciliary localization of ARL13B is independent of its interaction with IFT-B

We then addressed whether the ciliary localization of ARL13B is dependent on its interaction with the IFT-B complex, using the mutants described above. As shown in Fig. 3, tRFP-fused wild-type (WT) ARL13B (Fig. 3A) and its GTPase domain mutants (T35N, R79Q, ΔGD and Arf6GD; Fig. 3B–E, respectively) exhibited ciliary localization when expressed in hTERT-RPE1 cells (summarized in Fig. 2A), indicating that ARL13B localizes within cilia irrespective of its GTPase domain; this is in line with a previous report (Humbert et al., 2012). ARL13B(R200C), a Joubert syndrome-type mutant,

Journal of Cell Science (2017) 130, 563-576 doi:10.1242/jcs.197004

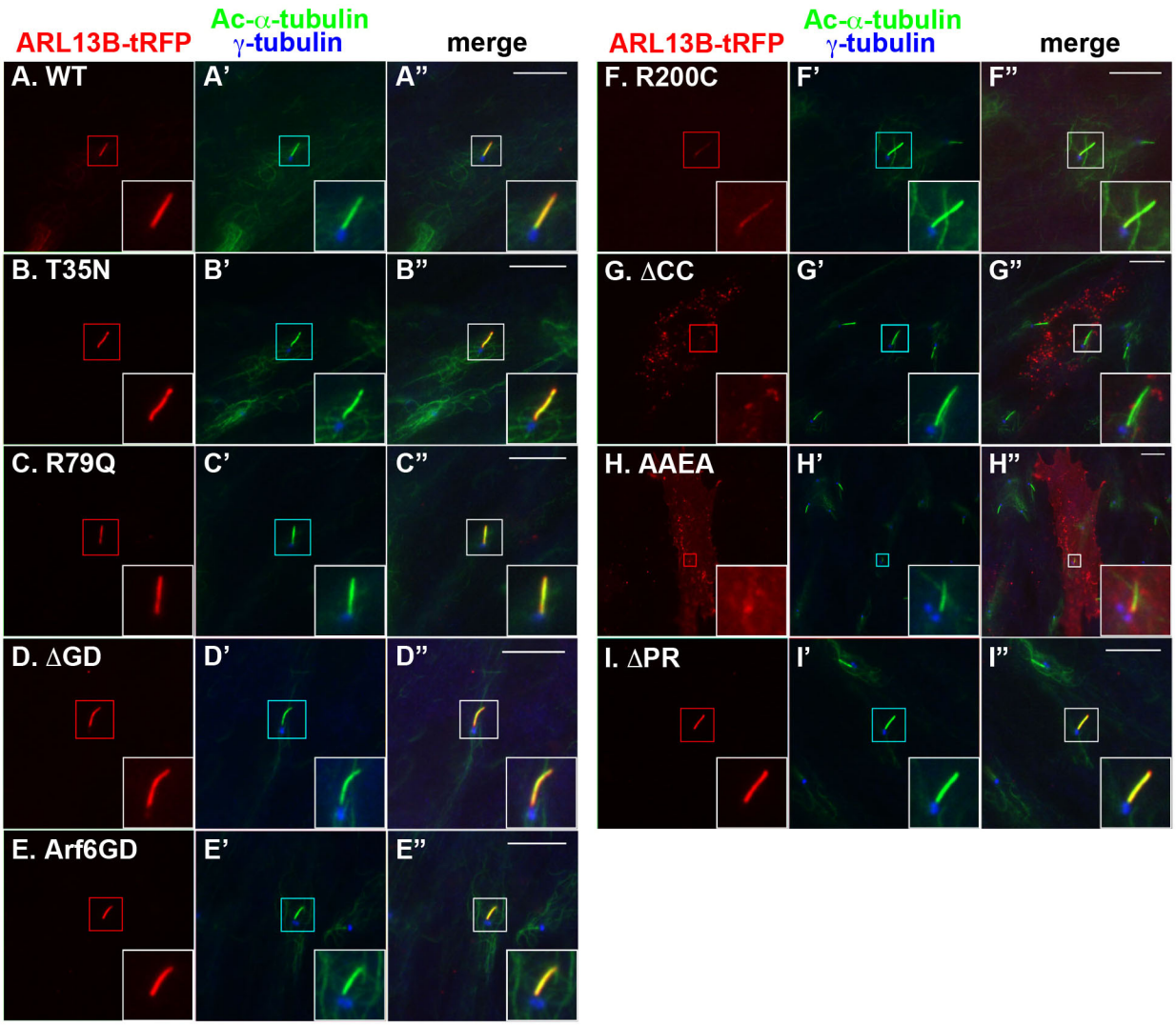

Fig. 3. Ciliary localization of ARL13B is dependent on its RVEP sequence but not on its interaction with IFT46–IFT56. hTERT-RPE1 cells expressing tRFP-fused ARL13B(WT) (A), ARL13B(T35N) (B), ARL13B(R79Q) (C), ARL13B(ΔGD) (D), ARL13B(Arf6GD) (E), ARL13B(R200C) (F), ARL13B(ΔCC) (G), ARL13B(AAEA) (H) or ARL13B(ΔPR) (I) were established as described in the Materials and Methods. The cells were serum starved for 24 h, and double immunostained for Ac-α-tubulin and γ-tubulin (A′–I′). Merged images are shown in A″–I″. Insets indicate enlarged images of the boxed regions (approximately 6 µm on a side). Scale bars: 10 µm.

was also localized in cilia (Fig. 3F). We also attempted to determine whether ARL13B(ΔCC) localizes to cilia, but our attempts have been unsuccessful so far, because this mutant fused to tRFP or other tags forms aggregates in the cytoplasm (Fig. 3G). As described above, the RVEP-to-AAEA mutation disrupted the ciliary localization of ARL13B (Fig. 3H); the ARL13B(AAEA) mutant appeared to be localized mainly at the plasma membrane as revealed by its even distribution throughout the cell, although it also formed aggregates in the cytoplasm. As shown in Fig. 3I, ARL13B(ΔPR), which cannot interact with IFT-B, retained the ability to localize in the cilium. Thus, the ciliary localization of ARL13B is dependent on the RVEP sequence, but independent of its GTP-bound state. Furthermore, it is unlikely that the IFT-B complex regulates the ciliary localization of ARL13B via a direct interaction.

ARL13B binding to INPP5E does not require its IFT-B-binding region

Next, to address the possibility that binding of ARL13B to IFT-B affects its binding to INPP5E, we examined whether ARL13B(WT) and its mutants interact with INPP5E by using the VIP assay as well as conventional immunoblotting analysis. A previous study reported that the T35N, R79Q or R200C mutations of ARL13B greatly reduced its binding ability to INPP5E (Humbert et al., 2012). Our VIP and immunoblotting experiments confirmed that point mutants of the GTPase domain, namely, ARL13B(T35N) and ARL13B(R79Q), retain weak but substantial binding ability to INPP5E (Fig. 2D,E, lanes 3 and 4).

Therefore, we then examined whether the ARL13B GTPase domain participates in the interaction of ARL13B with INPP5E, and found that neither the ΔGD or Arf6GD mutant can interact with INPP5E (Fig. 2D,E, lanes 5 and 6). Thus, the GTPase domain of ARL13B appears to be involved in the interaction of ARL13B and INPP5E, and point mutations in this domain attenuate but do not completely abolish the interaction. The R200C and ΔCC mutants of ARL13B did not bind to INPP5E (Fig. 2D,E, lanes 7 and 8), indicating that the CC region of ARL13B also participates in this interaction. On the other hand, we found that the AAEA and ΔPR mutants retain the ability to bind to INPP5E (Fig. 2D,E, lanes 9 and

Journal of Cell Science (2017) 130, 563-576 doi:10.1242/jcs.197004

10), indicating that the entry of ARL13B into cilia and its interaction with IFT-B are not necessarily required for its interaction with INPP5E.

ARL13B-KO cells accumulate IFT-A and IFT-B proteins at their ciliary tips

Previous histological and pathophysiological analyses of *hennin* mice and *scorpion* zebrafish unequivocally demonstrated the role of ARL13B in Hh signaling during development (Caspary et al., 2007; Duldulao et al., 2009; Larkins et al., 2011). However, neither of these studies addressed the role of ARL13B with respect to ciliary protein trafficking in detail. With the intent to further understand the roles of ARL13B in ciliary protein trafficking, we established *ARL13B*-KO hTERT-RPE1 cell lines by using a CRISPR/Cas9 system with our original modifications as described in the Materials and Methods and schematically shown in Fig. S1. To mitigate the risk of potential off-target cleavage associated with the CRISPR/Cas9 system, we used two different target sequences in exon 1 of the human *ARL13B* gene. Among a total of four *ARL13B*-KO cell lines that we established, we selected two cell lines established using distinct target sequences (#13b-1-2 and #13b-2-7) for the subsequent detailed analyses; the cell line #13b-1-2 has a 1-bp insertion (an A nucleotide) causing a frameshift in one allele and reverse integration of the donor knock-in vector in the other allele (Fig. S2A, lanes 5–7, and S2B), and the cell line #13b-2-7 has a 1-bp insertion (a C nucleotide) causing a frameshift in one allele and reverse integration of the donor knock-in vector in the other allele (Fig. S2A, lane 8–10, and Fig. S2C). Immunofluorescence analysis using the available polyclonal anti-ARL13B antibody, which was raised against a GST fusion protein of human ARL13B (BC094725, covering residues 1–20 and 128–428 of the ARL13B protein used in this study), confirmed that these KO cell lines lack ciliary ARL13B staining (Fig. 4A–C).

In control RPE1 cells, an antibody against the IFT-B subunit IFT88 labeled the base of cilia as well as weakly labeling the tip (Fig. 4D), consistent with previous studies (Follit et al., 2006; Jurczyk et al., 2004). In contrast, this anti-IFT88 antibody labeled the tip as well as the base of cilia in both *ARL13B*-KO cell lines (Fig. 4E,F, also see Fig. 4L).

Labeling using an antibody against the IFT-A subunit IFT140, was confined to the ciliary base in control RPE1 cells (Fig. 4G); note that the available anti-IFT140 antibody also labeled undetermined structures within the nucleus of RPE1 cells, as described by the manufacturer's website (http://www.ptglab.com/Products/IFT140-Antibody-17460-1-AP.htm). In both *ARL13B*-KO cell lines, predominant labeling for IFT140 was found around the tip as well as base of cilia (Fig. 4H,I, also see Fig. 4M), which was similar to that observed for IFT88 (Fig. 4E,F). These observations together indicate that retrograde trafficking of IFT particles containing IFT-A and IFT-B from the tip to base of cilia is likely to be prevented by the absence of ARL13B.

During the course of these experiments, we noted that *ARL13B*-KO cells exhibited a significant decrease in ciliary length, as compared with control RPE1 cells (Fig. 4J). This observation is compatible with observations of the cilia of *hennin* mice (Larkins et al., 2011) and a recent report showing that ARL13B overexpression results in an increase in ciliary length (Lu et al., 2015). We also noted that labeling with an antibody against acetylated α-tubulin (Ac-α-tubulin) along the cilium was weak in both *ARL13B*-KO cell lines relative to that found in control cells (Fig. 4K). This is in line with the original report of *hennin* mice showing that the ciliary axonemes of *hennin* mice are abnormal at the electron microscopic level (Caspary et al., 2007), although we did not further pursue this issue in this study.

ARL13B-KO cells exhibit no ciliary localization of INPP5E and increased ciliary localization of TULP3 and GPR161

We then compared the localization of INPP5E in control and *ARL13B*-KO RPE1 cells. In control cells, labeling with an anti-INPP5E antibody demonstrated an even distribution of INPP5E along cilia (Fig. 5A). By contrast, we did not detect any INPP5E labeling along the cilia or at the ciliary base in both *ARL13B*-KO cell lines (Fig. 5B,C).

While this study was in progress, Chávez et al. (2015) and Garcia-Gonzalo et al. (2015) independently reported that in cells derived from *INPP5E*$^{-/-}$ mice, phosphatidylinositol (4,5)-bisphosphate [PtdIns(4,5)P_2] is abnormally enriched on the ciliary membrane, resulting in increased ciliary localization of TULP3, which binds to PtdIns(4,5)P_2 through its Tubby-like domain (see Fig. 8), whereas PtdIns(4)*P* is found at high levels in normal cilia (reviewed in Nakatsu, 2015). The retention of TULP3 subsequently leads to abnormal ciliary accumulation of the IFT-A complex, which interacts with TULP3 (Mukhopadhyay et al., 2010), as well as the abnormal accumulation of GPR161, which is a G_s-protein-coupled orphan receptor that negatively regulates Hh signaling and which loses its ciliary localization in the absence of TULP3 (Mukhopadhyay et al., 2013). The increased ciliary localization, particularly at the ciliary tips, of IFT-A, TULP3 and GPR161 indicates that retrograde ciliary protein trafficking is diminished compared to anterograde trafficking. In view of our data showing that in *ARL13B*-KO cells IFT-A accumulates at ciliary tips (Fig. 4G–I) and INPP5E is not found in cilia (Fig. 5A–C), we then examined the various phenotypes of *ARL13B*-KO cells to compare them with those reported for *INPP5E*$^{-/-}$ cells.

INPP5E can convert PtdIns(4,5)P_2 into PtdIns(4)*P* (Conduit et al., 2012). We therefore examined the relative levels of these phosphoinositides in the cilia of control and *ARL13B*-KO cells using probes specific for these phosphoinositides, which were used in the study of Garcia-Gonzalo et al. (2015). As shown in Fig. 5D, the PtdIns(4)*P*-specific probe EGFP–2×P4M^{SidM} was enriched in the cilia of control RPE1 cells. Compared with the control cells, the ciliary level of the PtdIns(4)*P* probe was greatly reduced in *ARL13B*-KO cells (Fig. 5E,F). On the other hand, PtdIns(4,5)P_2 probed with PLCδ-PH–EGFP was detectable along the cilia of *ARL13B*-KO cells (Fig. 5H,I), whereas it was under the detection level in control cells (Fig. 5G). These observations suggest that the decrease in ciliary INPP5E levels in *ARL13B*-KO cells resulted in increased PtdIns(4,5)P_2 levels and decreased PtdIns(4)*P* levels, although there are technical limitations in experiments using such phospholipid probes.

Similar to the location observed for the IFT140 signals (Fig. 4G), EGFP–TULP3 signals were mainly found at the ciliary base in control cells (Fig. 5J), whereas they were observed along cilia particularly at ciliary tips in *ARL13B*-KO cells (Fig. 5K,L). The localization of EGFP–TULP3 in control and *ARL13B*-KO cells (Fig. 5J–L) was similar to that of IFT-A (Fig. 4G–I), which is consistent with the fact that TULP3 interacts with the IFT-A complex (Mukhopadhyay et al., 2010). Thus, the ciliary distribution of TULP3 in the absence of ARL13B is compatible with the increased levels of PtdIns(4,5)P_2 in cilia.

We then compared the localization of the Hh signaling pathway components Smoothened (SMO) and GPR161, in control and *ARL13B*-KO cells. Upon the binding of Hh to its receptor Patched, SMO gains entrance to cilia, whereas GPR161 exits cilia downstream of SMO activation (Briscoe and Thérond, 2013). In both control and

Journal of Cell Science (2017) 130, 563-576 doi:10.1242/jcs.197004

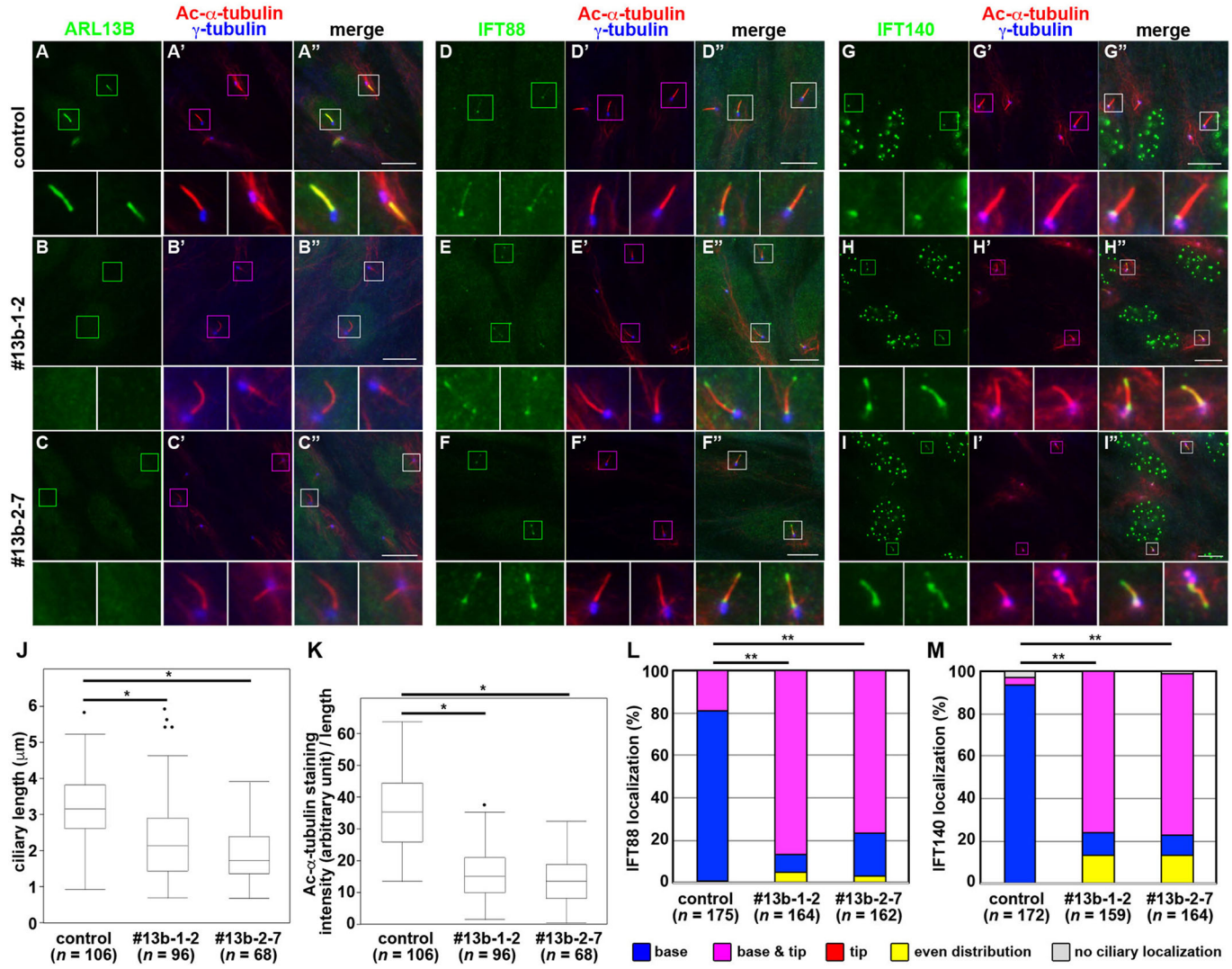

Fig. 4. Accumulation of IFT-A and IFT-B proteins at the ciliary tips in *ARL13B*-KO cells. Control RPE1 cells (A,D,G) or the *ARL13B*-KO cell lines #13b-1-2 (B,E,H) or #13b-2-7 (C,F,I) were serum-starved for 24 h and triple immunostained for either ARL13B (A–C), IFT88 (D–F) or IFT140 (G–I), Ac-α-tubulin, and γ-tubulin (A′–I′). Merged images are shown in A″–I″. Insets indicate enlarged images of the boxed regions. Scale bars: 10 µm. (J) Ciliary lengths of individual control and *ARL13B*-KO cells were measured and shown as box-and-whisker plots. The box represents the 25–75th percentiles [interquartile range (IQR)], and the median is indicated. The whiskers show the minimum and maximum within 1.5 × IQR from the 25th and 75th percentiles, respectively. Outliers are indicated with dots. The total numbers of ciliated cells observed (*n*) are shown. **P*<0.0001 (Student *t*-test). (K) The Ac-α-tubulin staining intensities (arbitrary units) for the length of a complete cilia in individual control and *ARL13B*-KO cells were estimated and expressed as a box-and-whisker plot as in J. The total numbers of ciliated cells observed (*n*) are shown. **P*<0.0001 (Student *t*-test). (L,M) Localization of IFT88 (L) and IFT140 (M) in individual control and *ARL13B*-KO cells was classified as 'ciliary base', 'ciliary tip', 'base and tip', 'even distribution within the cilium' and 'no ciliary localization', and the number in each category counted. The percentages of these populations are expressed as stacked bar graphs. Values are means of three independent experiments. In each set of experiments, 52–62 ciliated cells were observed, and the total numbers of ciliated cells observed (*n*) are shown. ***P*<0.001 (Pearson's χ^2 test).

ARL13B-KO RPE1 cells, SMO was rarely observed within cilia under basal conditions (Fig. 6A–C, also see Fig. 6M), but entered cilia when stimulated with Smoothened agonist (SAG) (Fig. 6D–F,M). It is, however, noteworthy that the population of cells with SMO at the ciliary tips was substantially increased in SAG-treated *ARL13B*-KO cells (Fig. 6M), although there was no significant difference in the percentage of cells with overall ciliary SMO staining between SAG-treated control and *ARL13B*-KO cells. These observations suggest that, although anterograde trafficking of SMO in response to SAG is not affected by ARL13B deficiency, its retrograde trafficking could be impaired.

GPR161 was evenly distributed along cilia in control cells under basal conditions (Fig. 6G). In striking contrast, GPR161 was substantially accumulated at ciliary tips in *ARL13B*-KO cells even under basal conditions (Fig. 6H,I, also see Fig. 6N). Furthermore, when stimulated with SAG, GPR161 exited the cilia in control cells (Fig. 6J), whereas a substantial amount remained at the ciliary tips of *ARL13B*-KO cells (Fig. 6K,L,N). Thus, retrograde trafficking of GPR161 downstream of SMO activation appears to be impaired by ARL13B deficiency.

The phenotypes of the *ARL13B*-KO RPE1 cells that we observed were similar to those reported for cells derived from *INPP5E*$^{-/-}$ mice (Chávez et al., 2015; Garcia-Gonzalo et al., 2015), indicating that ARL13B regulates the ciliary localization of INPP5E, which in turn regulates ciliary protein localization and Hh signaling by regulating membrane phosphoinositide composition.

Journal of Cell Science (2017) 130, 563-576 doi:10.1242/jcs.197004

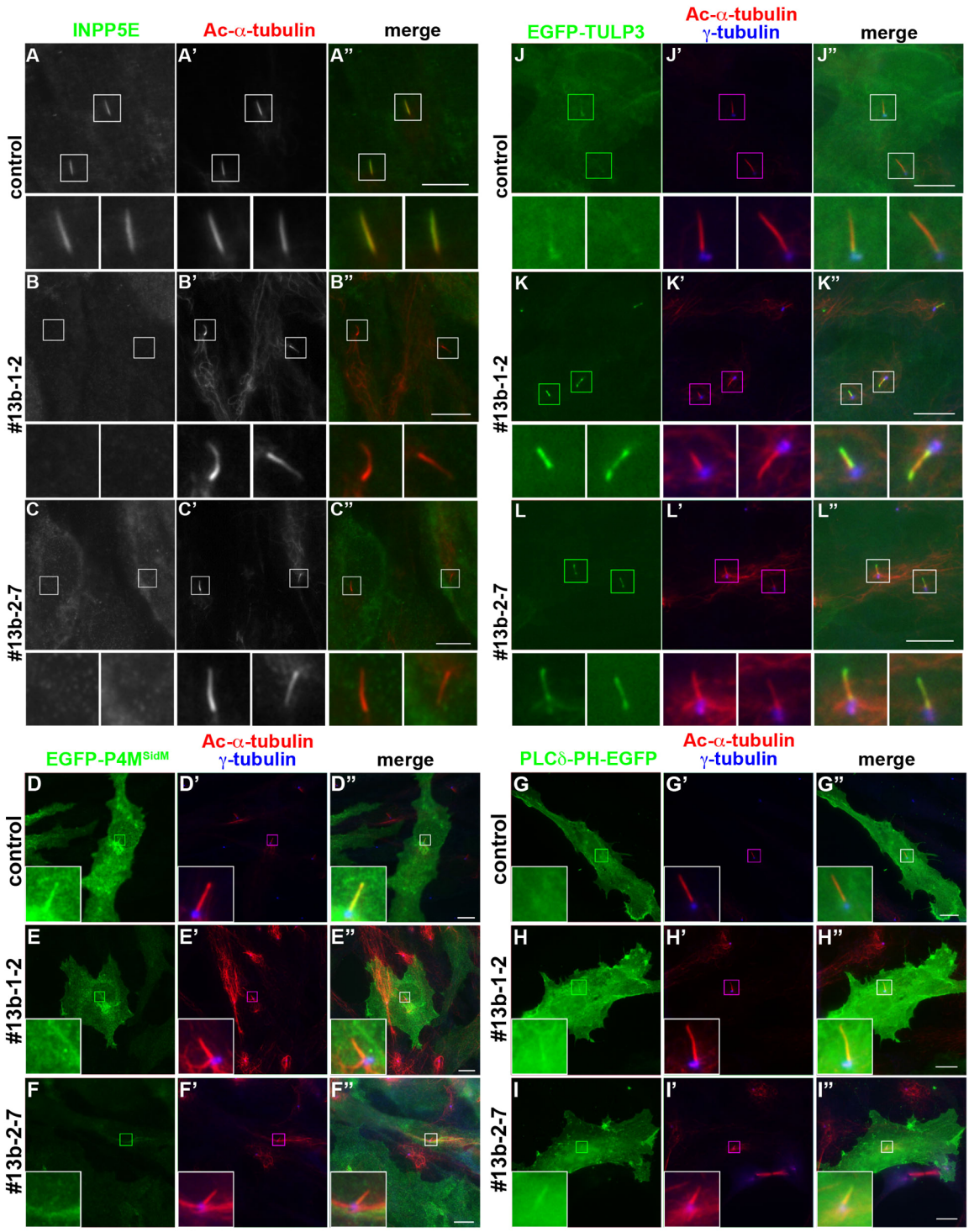

Fig. 5. Lack of INPP5E and PtdIns(4)*P*, and accumulation of PtdIns(4,5)P_2 and TULP3, in cilia of *ARL13B*-KO cells. (A–C) Control RPE1 cells (A) or the *ARL13B*-KO cell lines #13b-1-2 (B) or #13b-2-7 (C) were serum starved for 24 h and double immunostained for INPP5E (A–C) and Ac-α-tubulin (A′–C′). (D–L) Control RPE1 cells (D,G,J) or the *ARL13B*-KO cell lines #13b-1-2 (E,H, and K) or #13b-2-7 (F,I,L), stably expressing EGFP-2×P4M^{SidM} (D–F), or EGFP–TULP3 (J–L) were established as described in the Materials and Methods. PLCδ-PH-EGFP (G–I) was transiently expressed in the control and *ARL13B*-KO cells. These cells were serum starved for 24 h and double immunostained for Ac-α-tubulin and γ-tubulin (D′–L′). Merged images are shown in A″–C″ and D″–L″. Insets indicate enlarged images of the boxed regions. Scale bars: 10 µm.

Ciliary localization of INPP5E is independent of the interaction of ARL13B with the IFT-B complex

We next examined whether the ciliary localization of INPP5E in *ARL13B*-KO cells can be recovered by the exogenous expression of ARL13B and its mutants. When ARL13B(WT)–tRFP was exogenously expressed in the *ARL13B*-KO cell line #13b-1-2, the ciliary localization of INPP5E was completely restored (compare Fig. 7A,B). The #13b-1-2 cell line with the exogenous expression of

Journal of Cell Science (2017) 130, 563-576 doi:10.1242/jcs.197004

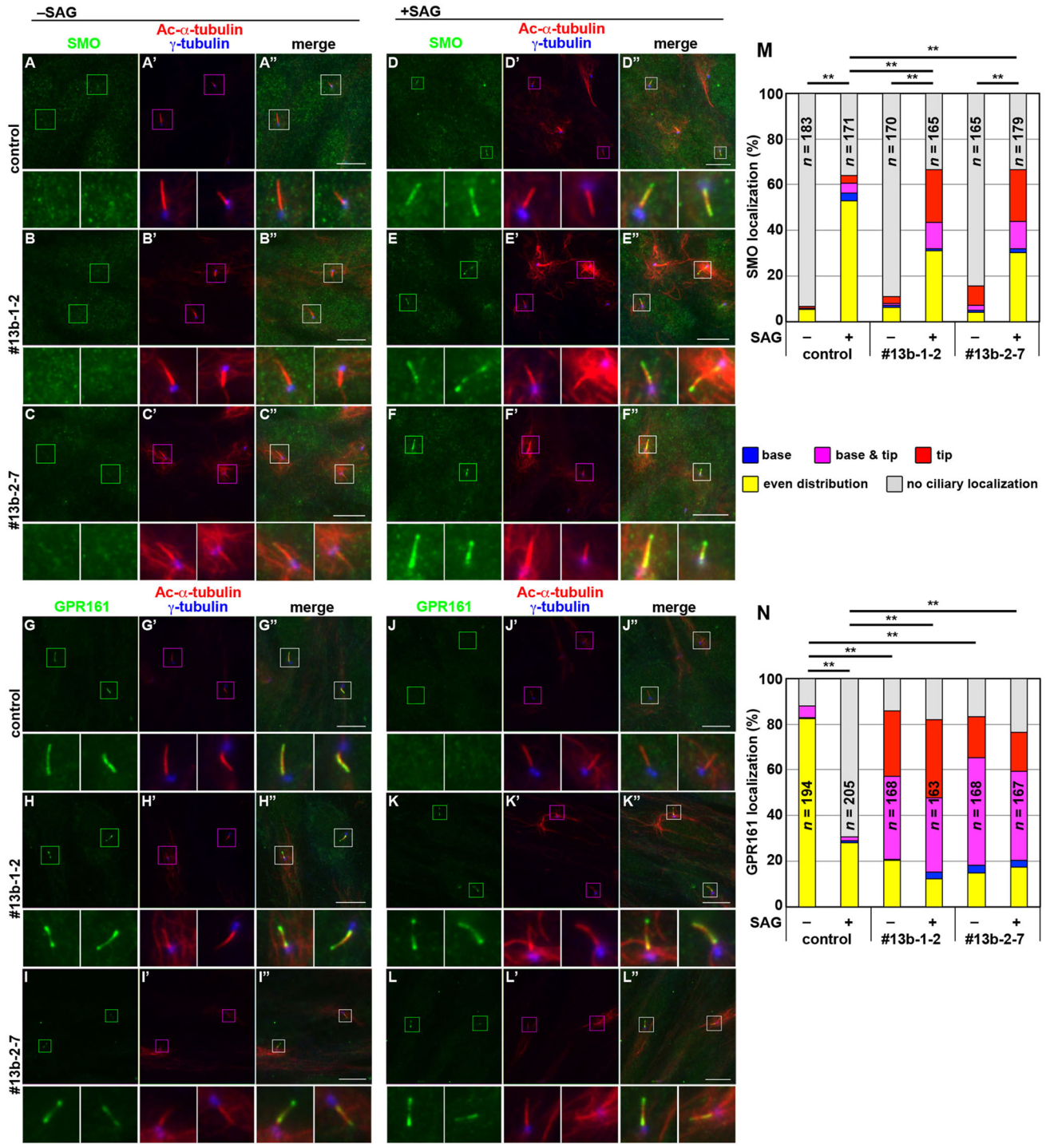

Fig. 6. Accumulation of GPR161 at the ciliary tips of *ARL13B*-KO cells. Control RPE1 cells (A,D,G,J), or the *ARL13B*-KO cell lines #13b-1-2 (B,E,H,K) or #13b-2-7 (C,F,I,L) were cultured for 24 h in the absence (–SAG) or presence (+SAG) of 200 nM SAG, and triple immunostained for either SMO (A–F) or GPR161 (G–L), Ac-α-tubulin and γ-tubulin (A′–L′). Merged images are shown in A″–L″. Insets indicate enlarged images of the boxed regions. Scale bars: 10 µm. (M,N) Localization of SMO (M) and GPR161 (N) in control and *ARL13B*-KO cells in the absence or presence of SAG was classified as described in the legend for Fig. 4L,M, and the number in each category counted. Percentages of these populations are expressed as stacked bar graphs. Values are means of three independent experiments. In each set of experiments, 50–77 ciliated cells were observed, and the total numbers of ciliated cells observed (*n*) are shown. ***P*<0.001 (Pearson's χ^2 test).

ARL13B(T35N), which retains a diminished but substantial ability to interact with INPP5E (Fig. 2D,E), exhibited a greatly reduced but substantial ciliary staining for INPP5E (Fig. 7C; also see Fig. 7G). In striking contrast, the exogenous expression of ARL13B(ΔGD)–tRFP did not restore the localization of INPP5E in cilia (Fig. 7D). ARL13B(AAEA), which can interact with INPP5E but cannot enter cilia, also failed to rescue the INPP5E ciliary localization defect (Fig. 7E,G), confirming that INPP5E enters cilia with the aid of ARL13B. Contrary to our initial hypothesis, ARL13B(ΔPR) restored the ciliary localization of INPP5E (Fig. 7F,G), in a

Journal of Cell Science

Journal of Cell Science (2017) 130, 563-576 doi:10.1242/jcs.197004

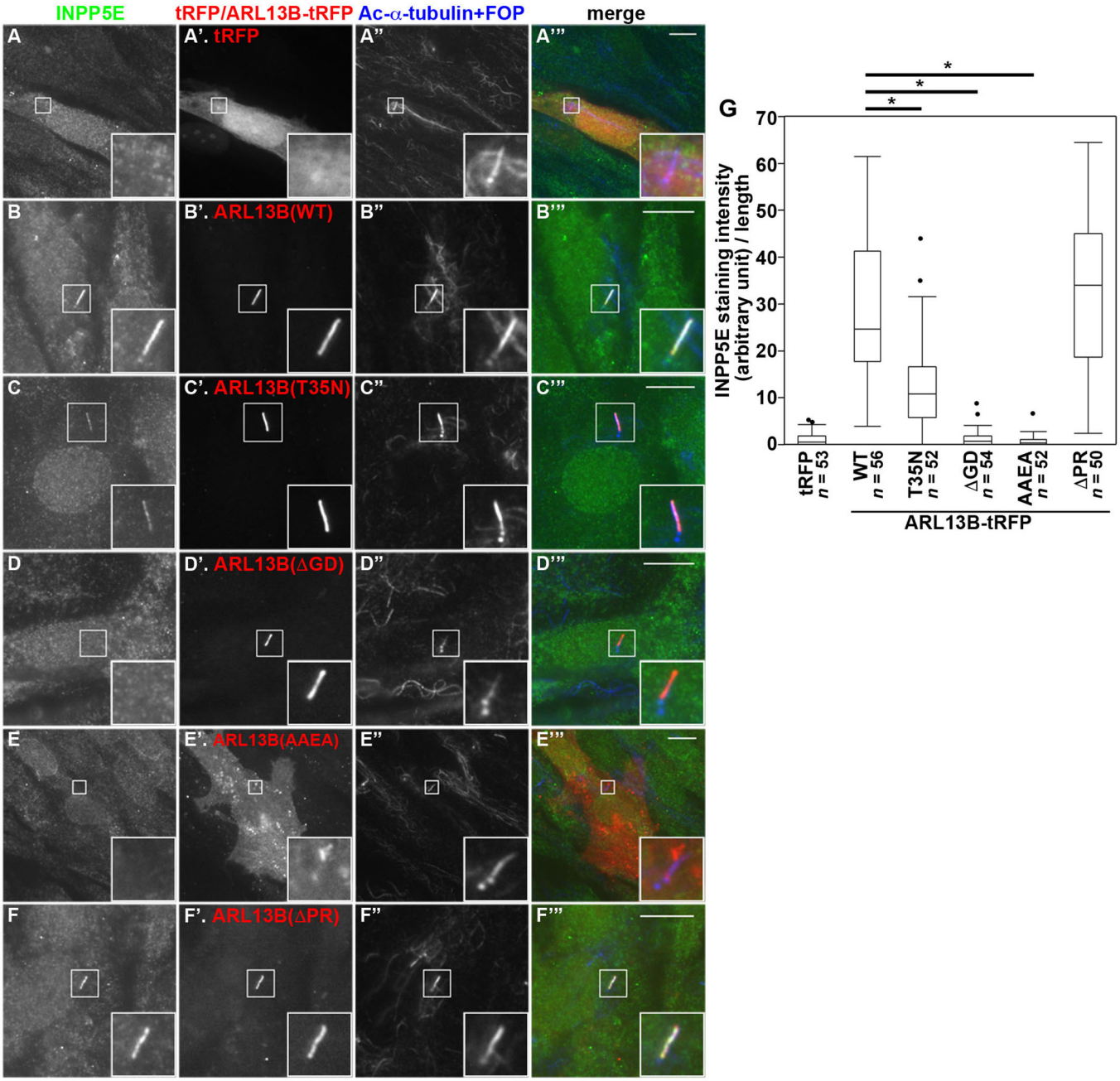

Fig. 7. Rescue of INPP5E ciliary localization in *ARL13B*-KO cells upon exogenous expression of wild-type and mutant ARL13B. The #13b-1-2 cell line expressing tRFP (A′), tRFP-fused ARL13B(WT) (B′), ARL13B(T35N) (C′), ARL13B(ΔGD) (D′), ARL13B(AAEA) (E′), or ARL13B(ΔPR) (F′) were serum starved for 24 h and double immunostained for INPP5E (A–F) and Ac-α-tubulin+FOP (FGFR1OP) (A″–F″). FOP is a marker for the basal body. Merged images are shown in A‴–F‴. Insets indicate enlarged images of the boxed regions. Scale bars: 10 µm. (G) The INPP5E staining intensities (arbitrary units) for the length of a complete cilia in individual *ARL13B*-KO cells expressing Arl13b constructs indicated were estimated and expressed as box-and-whisker plots. The box represents the 25–75th percentiles [interquartile range (IQR)], and the median is indicated. The whiskers show the minimum and maximum within 1.5 × IQR from the 25th and 75th percentiles, respectively. Outliers are indicated with dots. The total numbers of ciliated cells observed (*n*) are shown. **P*<0.0001 (Student *t*-test).

similar manner to ARL13B(WT) (Fig. 7B). These observations indicate that INPP5E enters cilia through its continuous interaction with ARL13B, but independently of the interaction of ARL13B with the IFT-B complex, although IFT-B is essential for the anterograde transport of other ciliary proteins (Sung and Leroux, 2013).

Similarly, the exit of GPR161 from cilia in response to SAG (Fig. S3A–L) and the retrograde transport of IFT-B (Fig. S3M–R) were restored by the exogenous expression of ARL13B(WT), ARL13B(T35N) or ARL13B(ΔPR), but not by that of ARL13B (ΔGD) or ARL13B(AAEA). Thus, all the examined defects in *ARL13B*-KO cells can be rescued by the ARL13B-mediated ciliary localization of INPP5E.

DISCUSSION

In this study, we identified subunits of the IFT-B complex that are responsible for its interaction with ARL13B by taking advantage of the VIP assay that we originally established; ARL13B interacts with

Journal of Cell Science (2017) 130, 563-576 doi:10.1242/jcs.197004

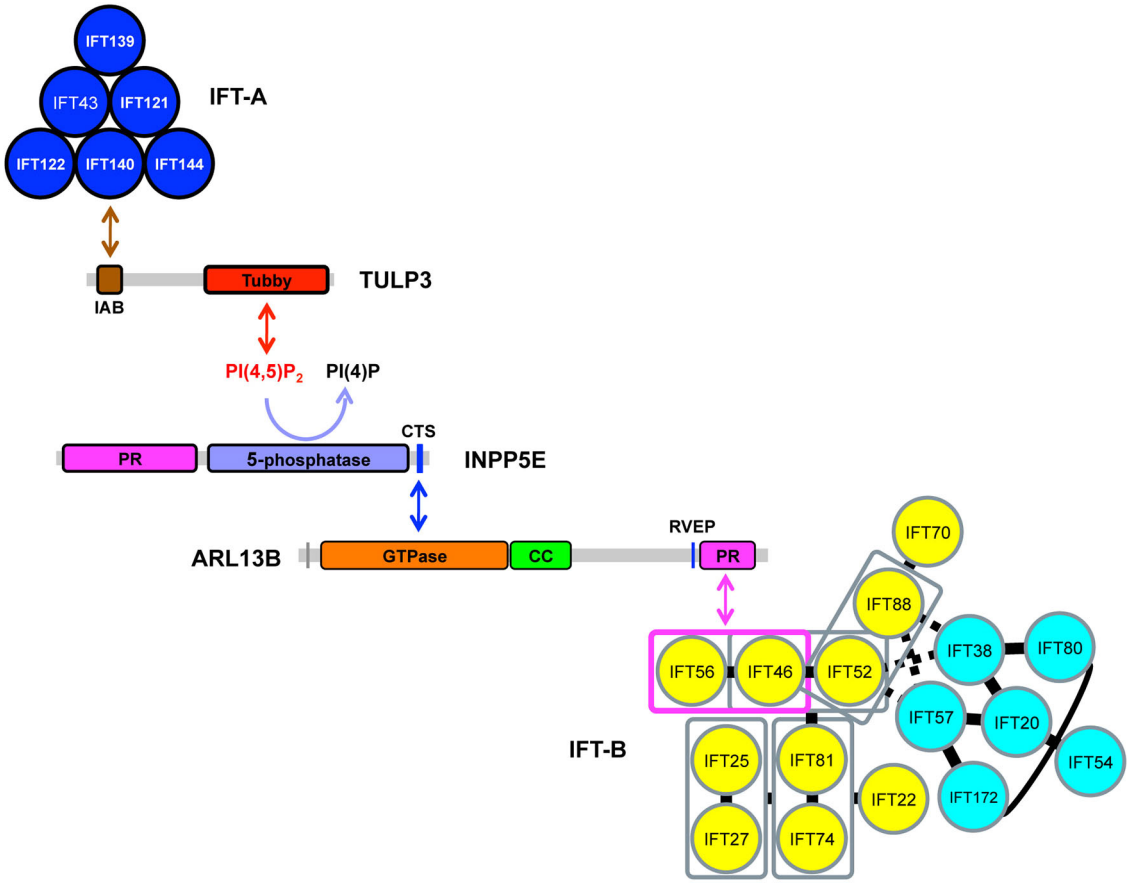

Fig. 8. Schematic representation of the interaction pathway involving ARL13B–INPP5E. This scheme represents how the ARL13B–INPP5E interaction is involved in ciliary protein trafficking. For more details, see the Discussion. IAB, IFT-A–binding sequence; 5-phosphatase, 5-phosphatase domain; CTS, ciliary targeting sequence.

a heterodimer of IFT46 and IFT56 through its C-terminal region (Fig. 8). Because the IFT-B complex generally mediates anterograde protein trafficking (from the base to the tip) within cilia (Sung and Leroux, 2013), we addressed the possibility that the ciliary localization of ARL13B is dependent on its direct interaction with the IFT-B complex. However, mutation of the ciliary-targeting sequence (RVEP) of ARL13B to AAEA did not affect its interaction with IFT-B (Fig. 2B,C). Furthermore, ARL13B(ΔPR), which fails to interact with the IFT-B subunits (Fig. 2B,C), is localized within cilia (Fig. 3I). These results demonstrate that the ciliary localization of ARL13B is independent of its interaction with the IFT-B complex.

We next analyzed another possibility, namely that ARL13B regulates the ciliary localization of its effectors through interaction with the IFT-B complex. INPP5E, as well as ARL13B, is encoded by a causative gene of Joubert syndrome, and is localized in cilia in an ARL13B-dependent manner. The interaction of ARL13B with INPP5E involves its GTPase domain and CC region (Fig. 2D,E). In *ARL13B*-KO cells, INPP5E cannot localize to cilia (Fig. 5A–C). Furthermore, TULP3, the IFT-A and IFT-B complexes, and GPR161 accumulate at the ciliary tips of *ARL13B*-KO cells, suggesting inhibition of retrograde ciliary protein trafficking (Figs 4–6). This phenotype resembled the reported phenotypes of cells derived from *INPP5E*$^{-/-}$ mice (Chávez et al., 2015; Garcia-Gonzalo et al., 2015; Nakatsu, 2015). As INPP5E is a phosphoinositide 5-phosphatase, the absence of INPP5E within the cilia of *ARL13B*-KO cells causes an increase in the PtdIns(4,5)P_2 levels in ciliary membranes. TULP3 has a PtdIns(4,5)P_2-binding domain and interacts with the IFT-A complex (Mukhopadhyay et al., 2010) (see Fig. 8), which mediates the retrograde trafficking of ciliary proteins (Sung and Leroux, 2013). GPR161 is a G_s-protein-coupled receptor that negatively regulates Hh signaling, and localizes to cilia in a TULP3-dependent manner (Mukhopadhyay et al., 2013). Thus, ciliary TULP3 accumulation in turn leads to ciliary retention of the IFT-A complex and its cargo protein GPR161, which suppresses Hh signaling. These results together demonstrate that essentially the same molecular mechanism is likely to be responsible for the etiology of JBTS, which is caused by mutations in the *ARL13B* (*JBTS8*) and *INPP5E* (*JBTS1*) genes.

The increased ciliary localization, particularly at the ciliary tips, of various proteins, including IFT-A plus TULP3, IFT-B and GPR161, in *ARL13B*-KO cells suggests alternative possibilities for the changes in ciliary protein trafficking, namely, increased anterograde trafficking and/or ciliary entry, or impaired retrograde trafficking. We think that the latter possibility is more likely for the following reasons: (1) ciliary localization of SMO was not increased under basal conditions in *ARL13B*-KO cells, and was increased to a similar extent upon SAG treatment of control and *ARL13B*-KO cells, suggesting that anterograde trafficking or ciliary entry of SMO is not enhanced by ARL13B deficiency; and (2) GPR161 was significantly accumulated within cilia under basal conditions in *ARF13B*-KO cells as compared with control cells, and could not exit cilia in response to SAG treatment, suggesting impaired retrograde trafficking.

Recently, Gotthardt et al. (2015) reported that ARL13B serves as a GEF for ARL3, which in turn binds to and stimulates release of PDE6D from C-terminally prenylated proteins, including INPP5E,

Journal of Cell Science (2017) 130, 563-576 doi:10.1242/jcs.197004

which are then allowed to enter cilia (Fansa et al., 2016; Ismail et al., 2011). Furthermore, Fansa et al. reported that treatment of cells with ARL3 siRNA caused substantial loss of the dominant ciliary localization of GFP-tagged INPP5E and its redistribution to between the cilia and the plasma membrane (Fansa et al., 2016). It is, therefore, possible that displacement of INPP5E from cilia observed in *ARL13B*-KO cells resulted indirectly from the deficiency of an ARL3 GEF, namely ARL13B. In addition to the indirect mechanism, however, the data presented in this study indicate that the direct interaction of ARL13B with INPP5E determines the ciliary INPP5E localization. This is supported by previous data of Humbert et al. (2012) showing (1) that INPP5E constructs lacking the ARL13B-binding sequence but retaining the C-terminal CaaX motif for prenylation cannot enter cilia; (2) reciprocally, an INPP5E mutant lacking the C-terminal CaaX motif but retaining the ARL13B-binding sequence can enter cilia; and (3), treatment of cells with siRNA for ARL13B, but not that for ARL3, abolishes ciliary localization of INPP5E. Thus, these data are compatible with our view that ARL13B binding is directly involved in ciliary localization of INPP5E, and suggest that PDE6D is required for efficient extraction of prenylated INPP5E from membranes but is not directly required for its ciliary targeting.

We discovered that both the IFT-B complex as well as the IFT-A complex accumulate at the ciliary tips of *ARL13B*-KO cells (Fig. 4D–F), and that the exogenous expression of ARL13B (ΔGD) or ARL13B(AAEA), which cannot restore the ciliary localization of INPP5E, fails to rescue the abnormal accumulation of the IFT-B complex. On the other hand, we found that the exogenous expression of ARL13B(ΔPR), which cannot interact with the IFT-B complex, rescues the abnormal accumulation of IFT-B (Fig. S3M–R). These observations indicate that the abnormal accumulation of IFT-B in *ARL13B*-KO cells did not result from the absence of the interaction of IFT-B with ARL13B, but resulted from an increase in PtdIns(4,5)P_2 levels in ciliary membranes and the consequent ciliary accumulation of the IFT-A complex via TULP3–PtdIns(4,5)P_2 interaction.

By performing rescue experiments in *ARL13B*-KO cells (Fig. 7), we showed that the ciliary localization of INPP5E was restored by the exogenous expression of ARL13B(WT) or ARL13B(ΔPR), but not by that of ARL13B(ΔGD) or ARL13B(AAEA). Thus, the ARL13B(ΔPR) mutant, which fails to interact with IFT-B subunits, retains the ability to localize in cilia and to mediate the ciliary localization of INPP5E. These results indicate that the ciliary localization of INPP5E is independent of the interaction of ARL13B with the IFT-B complex. Therefore, identification of the actual physiological events that the ARL13B–IFT-B interaction participates in is an issue that should be addressed in future studies; one possibility is that some unknown cargo proteins can bind to the IFT-B complex with the aid of ARL13B. Another issue to be addressed is what determines the ciliary localization of ARL13B, which is probably mediated through an interaction of a protein with the ciliary-targeting sequence RVEP. One candidate is the nuclear import machinery, as there are lines of evidence suggesting that components of the nuclear import machinery, including the Ran GTPase and importins, are involved in the entry of proteins through the transition zone into cilia (Dishinger et al., 2010; Hurd et al., 2011). It will also be interesting to investigate whether transition zone proteins, which when mutated result in ciliopathies including Joubert syndrome (Garcia-Gonzalo et al., 2011; Warburton-Pitt et al., 2014), are directly involved in the ciliary entry of ARL13B. Recently, Slaats et al. reported that ARL13B and INPP5E are markedly reduced in the cilia of fibroblasts derived from JBTS patients in which the *MKS1* gene is mutated (Slaats et al., 2016). Because MKS1 functions in the transition zone by forming a complex with other proteins (Chih et al., 2012; Garcia-Gonzalo et al., 2011), MKS1 or other associated proteins are candidate regulators for the ciliary entry of ARL13B.

MATERIALS AND METHODS

Plasmids

The construction of expression vectors for IFT-B proteins were as described previously (Katoh et al., 2016). The construction of an expression vector for ARL13B was also described previously (Hori et al., 2008). The mutant constructs of ARL13B used in this study are listed in Table S1. Human INPP5E cDNA (a kind gift from Junya Hasegawa and Tamotsu Yoshimori, Osaka University, Japan) (Hasegawa et al., 2016) was subcloned into the pCAG-mCherry-C vector. Plasmid vectors for the production of lentiviral vectors (Thomas et al., 2009) were kindly provided by Peter McPherson (McGill University, Canada).

Antibodies and reagents

Antibodies used in this study are listed in Table S2. GST-tagged anti-GFP Nb prebound to glutathione–Sepharose 4B beads were prepared as described previously (Katoh et al., 2015). SAG was purchased from Enzo Life Sciences, and Polyethylenimine Max was purchased from Polysciences.

Establishment of KO cell lines using the CRISPR/Cas9 system

The basis of the strategy to establish *ARL13B*-KO cell lines (Fig. S1) followed the strategy described by Kimura et al. (2014), albeit with our original modifications as will be described elsewhere in detail. pSpCas9 (BB)-2A-Puro (Addgene plasmid, #48139) (Ran et al., 2013) was used as the vector to generate a single guide RNA (sgRNA). The sgRNA sequences targeting human *ARL13B* (#1, 5′-GCTGCGGCTGGTTCAAGCGG-3′; and #2, 5′-TGATGGCCAGTTGCTGCGGC-3′) were chosen using CRISPR Design (http://crispr.mit.edu/) (also see Table S3). The donor vector for knock-in includes the *ARL13B*-targeting sgRNA sequence followed by a protospacer adjacent motif (PAM) sequence and two reporter genes: TagBFP (tBFP) with a triplicated nuclear localization signal (NLS), and a neomycin-resistance gene (Neo). Human retinal pigment epithelial hTERT-RPE1 cells (ATCC, CRL-4000) cultured to ∼3.0×10^5 cells on a 12-well plate were transfected with 1 µg of the pSpCas9(BB)-2A-Puro and 0.25 µg of the donor knock-in vector using X-tremeGENE9 DNA Transfection Reagent (Roche Applied Science). After selection in medium containing G418 (600 µg/ml), the colonies with nuclear tBFP fluorescence were isolated. To check the *ARL13B* genes, genomic DNA was extracted from the isolated cells and subjected to PCR using KOD FX Neo DNA polymerase (TOYOBO). Three sets of primers (Table S3) were used to distinguish the following three states of integration of the donor vector: forward integration, reverse integration, and no integration with a small insertion or deletion (see Fig. S1). Direct sequencing of the PCR products confirmed the KO of both alleles of the *ARL13B* gene in the cells, with integration of the donor vector, or small deletions or insertions causing a frameshift.

VIP assay

VIP assays were performed as described previously (Katoh et al., 2015, 2016). Briefly, HEK293T cells (kindly provided by Hiroyuki Takatsu, Kyoto University) cultured to ∼1.6×10^6 cells on a 6-well plate in Dulbecco's modified Eagle's medium (DMEM) with high glucose (Nacalai Tesque) supplemented with 5% fetal bovine serum (FBS) were transfected with the EGFP and the tRFP or mChe fusion constructs (2 µg each) using Polyethylenimine Max (20 µg). After 24 h, the transfected cells were lysed in 250 µl of lysis buffer (50 mM HEPES-KOH pH 7.4, 100 mM KCl, 5 mM NaCl, 3 mM $MgCl_2$, 0.5% Triton X-100, 10% glycerol and 1 mM DTT) containing an EDTA-free protease inhibitor cocktail (Nacalai Tesque). The cell lysates were incubated with 5 µl of GST-fused anti-GFP Nb beads at 4°C for 1 h. After washing three times with lysis buffer, the

Journal of Cell Science (2017) 130, 563-576 doi:10.1242/jcs.197004

precipitated beads were observed using an all-in-one-type fluorescence microscope (Biozero BZ-8000, Keyence) with a 20×0.75 NA objective lens under constant conditions (sensitivity ISO 400, exposure of 33 ms for green fluorescence; and sensitivity ISO 800, exposure of 100 ms for red fluorescence) unless otherwise stated.

Preparation of cells stably expressing ARL13B–tRFP, EGFP–2×P4M^{SidM} and EGFP–TULP3

Recombinant lentiviral vectors were prepared as described previously (Takahashi et al., 2012). Briefly, a pRRLsinPPT vector carrying the gene of interest was transfected into HEK293T cells using Polyethylenimine Max along with packaging plasmids (pRSV-REV, pMD2.g, and pMDLg/pRRE). After changing the medium 8 h after transfection, culture media containing the lentiviral vector were collected after 24, 36 and 48 h, passed through a 0.45-µm filter (Sartorius), and centrifuged at 32,000 ***g*** at 4°C for 4 h using an R15A rotor and Himac CR22G centrifuge (Hitachi Koki, Japan). The precipitated viral particles were resuspended in DMEM/F-12 (Nacalai Tesque) and stored at −80°C until use.

Control and *ARL13B*-KO hTERT-RPE1 cells expressing ARL13B(WT)-tRFP or its mutants were prepared by adding the lentiviral suspension into the medium 24 h before cell fixation in every experiment. Cells stably expressing EGFP–TULP3 were generated by infection of the lentiviral vector with a range of dilutions and identified from the expression level of EGFP–TULP3. These cells were used for immunofluorescence analyses.

Control and *ARL13B*-KO hTERT-RPE1 cells stably expressing EGFP-2×P4M^{SidM} were prepared using an episomal expression vector system. The 2×P4M^{SidM} cDNA (Addgene plasmid #51472) (Hammond et al., 2014) was cloned into the pEBMulti-Ble-EGFP episomal vector (Wako Pure Chemical Industries). Control and *ARL13B*-KO cells transfected with pEBMulti-Ble-EGFP-2×P4M^{SidM} were selected in medium containing Zeocin (25 µg/ml) for ∼14 days. These cells were used for immunofluorescence analyses.

Immunofluorescence analysis

hTERT-RPE1 cells were cultured in DMEM/F-12 supplemented with 10% FBS and 0.348% sodium bicarbonate. To induce ciliogenesis, cells were grown to 100% confluence on coverslips, and starved for 24 h in starvation medium [Opti-MEM (Invitrogen) containing 0.2% bovine serum albumin]. For the SAG experiments, cells were cultured for an additional 24 h in fresh starvation medium containing DMSO (denoted −SAG) or 200 nM SAG (denoted +SAG). Expression vectors were transfected into the cells using X-tremeGENE9 DNA Transfection Reagent (Roche Applied Science).

Immunofluorescence analysis was performed as described previously (Katoh et al., 2016; Takahashi et al., 2012, 2011). Cells were fixed with 3% paraformaldehyde at 37°C for 15 min, washed three times with phosphate-buffered saline (PBS), quenched with 50 mM NH_4Cl for 10 min, washed three times with PBS, permeabilized with 0.1% Triton X-100 for 5 min, and washed three times with PBS. For the detection of endogenous INPP5E, cells were permeabilized with 0.1% saponin in primary and secondary antibody solution. For the detection of endogenous GPR161 and IFT88, cells were fixed and permeabilized with 3% paraformaldehyde at 37°C for 5 min and subsequently in 100% methanol for 5 min at −20°C, and washed three times with PBS. For detection of endogenous IFT140, cells were fixed and permeabilized with 100% methanol for 5 min at −20°C, and washed three times with PBS. The fixed and permeabilized cells were blocked with 10% FBS, and stained with antibodies diluted in 5% FBS. The stained cells were observed using an Axiovert 200M microscope (Carl Zeiss).

For quantification analysis, all images were acquired under the same setting and imported as TIFF files using ImageJ software. A ROI was constructed by drawing a line of 3-point width along the ciliary signal of Ac-α-tubulin using a segmented line tool. To correct for local background intensity, the ROI was duplicated and dragged to a nearby region. Intensities of Ac-α-tubulin staining were calculated by subtraction of the background value, followed by normalization to the ciliary length. Statistical analyses were performed using JMP Pro 12 software (SAS Institute).

Acknowledgements

We are grateful to Junya Hasegawa and Tamotsu Yoshimori for providing the INPP5E cDNA, and Peter McPherson for providing plasmids for lentiviral production. We also thank Helena Akiko Popiel for critical reading of the manuscript.

Competing interests

The authors declare no competing or financial interests.

Author contributions

S.N. and Y.K. designed and performed the experiments, and prepared the manuscript; M.T., S.M., S.T., and T.F. performed the experiments; K.K. designed the experiments; and K.N. designed the experiments and prepared the manuscript.

Funding

This work was supported in part by Grants-in-Aid for Scientific Research on Innovative Areas 'Cilia and Centrosome' from the Ministry of Education, Culture, Sports, Science, and Technology, Japan (grant numbers 25113514 and 15H01211 to K.N.); grants from the Japan Society for the Promotion of Science (JSPS) (grant numbers 22390013, 15H04370 and 15K14456 to K.N., and 25860044 and 15K07929 to Y.K.); and grants from the Uehara Memorial Foundation to K.N. and from the Takeda Science Foundation to Y.K. S.N. was supported by a JSPS Research Fellowship for Young Scientists.

Supplementary information

Supplementary information available online at
http://jcs.biologists.org/lookup/doi/10.1242/jcs.197004.supplemental

References

Bhogaraju, S., Cajánek, L., Fort, C., Blisnick, T., Weber, K., Taschner, M., Mizuno, N., Lamla, S., Bastin, P., Nigg, E. A. et al. (2013). Molecular basis of tubulin transport within the cilium by IFT74 and IFT81. *Science* **341**, 1009-1012.

Boldt, K., van Reeuwijk, J., Lu, Q., Koutroumpas, K., Nguyen, T.-M. T., Texier, Y., van Beersum, S. E. C., Horn, N., Willer, J. R., Mans, D. A. et al. (2016). An organelle-specific protein landscape identifies novel diseases and molecular mechanisms. *Nat. Commun.* **7**, 11491.

Briscoe, J. and Thérond, P. P. (2013). The mechanisms of Hedgehog signalling and its roles in development and disease. *Nat. Rev. Mol. Cell Biol.* **14**, 416-429.

Brown, J. M. and Witman, G. B. (2014). Cilia and diseases. *BioScience* **64**, 1126-1137.

Cantagrel, V., Silhavy, J. L., Bielas, S. L., Swistun, D., Marsh, S. E., Bertrand, J. Y., Audollent, S., Attié-Bitach, T., Holden, K. R., Dobyns, W. B. et al. (2008). Mutations in the cilia gene ARL13B lead to the classical form of Joubert syndrome. *Am. J. Hum. Genet.* **83**, 170-179.

Caspary, T., Larkins, C. E. and Anderson, K. V. (2007). The graded response to Sonic hedgehog depends on cilia architecture. *Dev. Cell* **12**, 767-778.

Cevik, S., Sanders, A. A. W. M., Van Wijk, E., Boldt, K., Clarke, L., van Reeuwijk, J., Hori, Y., Horn, N., Hetterschijt, L., Wdowicz, A. et al. (2013). Active transport and diffusion barriers restrict Joubert Syndrome-associated ARL13B/ARL-13 to an Inv-like ciliary membrane subdomain. *PLOS Genet.* **9**, e1003977.

Chávez, M., Ena, S., Van Sande, J., de Kerchove d'Exaerde, A., Schurmans, S. and Schiffmann, S. N. (2015). Modulation of ciliary phosphoinositide content regulates trafficking and sonic hedgehog signaling output. *Dev. Cell* **34**, 338-350.

Chih, B., Liu, P., Chinn, Y., Chalouni, C., Komuves, L. G., Hass, P. E., Sandoval, W. and Peterson, A. S. (2012). A ciliopathy complex at the transition zone protects the cilia as a privileged membrane domain. *Nat. Cell Biol.* **14**, 61-72.

Conduit, S. E., Dyson, J. M. and Mitchell, C. A. (2012). Inositol polyphosphate 5-phosphatases; new players in the regulation of cilia and ciliopathies. *FEBS Lett.* **586**, 2846-2857.

Cortés, C. R., Metzis, V. and Wicking, C. (2015). Unmasking the ciliopathies: craniofacial defects and the primary cilium. *WIREs Dev. Biol.* **4**, 637-653.

Dishinger, J. F., Kee, H. L., Jenkins, P. M., Fan, S., Hurd, T. W., Hammond, J. W., Truong, Y. N.-T., Margolis, B., Martens, J. R. and Verhey, K. J. (2010). Ciliary entry of the kinesin-2 motor KIF17 is regulated by importin-β2 and RanGTP. *Nat. Cell Biol.* **12**, 703-710.

Duldulao, N. A., Lee, S. and Sun, Z. (2009). Cilia localization is essential for in vivo functions of the Joubert syndrome protein Arl13b/Scorpion. *Development* **136**, 4033-4042.

Fansa, E. K., Kösling, S. K., Zent, E., Wittinghofer, A. and Ismail, S. (2016). PDE6δ-mediated sorting of INPP5E into the cilium is determined by cargo-carrier affinity. *Nat. Commun.* **7**, 11366.

Follit, J. A., Tuft, R. A., Fogarty, K. E. and Pazour, G. J. (2006). The intraflagellar transport protein IFT20 is associated with the Golgi complex and is required for cilia assembly. *Mol. Biol. Cell* **17**, 3781-3792.

Garcia-Gonzalo, F. R., Corbit, K. C., Sirerol-Piquer, M. S., Ramaswami, G., Otto, E. A., Noriega, T. R., Seol, A. D., Robinson, J. F., Bennett, C. L., Josifova, D. J. et al. (2011). A transition zone complex regulates mammalian ciliogenesis and ciliary membrane composition. *Nat. Genet.* **43**, 776-784.

Garcia-Gonzalo, F. R., Phua, S. C., Roberson, E. C., Garcia, G., III, Abedin, M., Schurmans, S., Inoue, T. and Reiter, J. F. (2015). Phosphoinositides regulate ciliary protein trafficking to modulate hedgehog signaling. *Dev. Cell* **34**, 400-409.
Geister, K. A. and Camper, S. A. (2015). Advances in skeletal dysplasia genetics. *Annu. Rev. Genomics Hum. Genet.* **16**, 199-227.
Geng, L., Okuhara, D., Yu, Z., Tian, X., Cai, Y., Shibazaki, S. and Somlo, S. (2006). Polycystin-2 traffics to cilia independently of polycystin-1 by using an N-terminal RVxP motif. *J. Cell Sci.* **119**, 1383-1395.
Gotthardt, K., Lokaj, M., Koerner, C., Falk, N., Gießl, A. and Wittinghofer, A. (2015). A G-protein activation cascade from Arl13B to Arl3 and implications for ciliary targeting of lipidated proteins. *Elife* **4**, e11859.
Hammond, G. R. V., Machner, M. P. and Balla, T. (2014). A novel probe for phosphatidylinositol 4-phosphate reveals multiple pools beyond the Golgi. *J. Cell Biol.* **205**, 113-126.
Hasegawa, J., Iwamoto, R., Otomo, T., Nezu, A., Hamasaki, M. and Yoshimori, T. (2016). Autophagosome-lysosome fusion in neurons requires INPP5E, a protein associated with Joubert syndrome. *EMBO J.* **35**, 1853-1867.
Higginbotham, H., Eom, T.-Y., Mariani, L. E., Bachleda, A., Hirt, J., Gukassyan, V., Cusack, C. L., Lai, C., Caspary, T. and Anton, E. S. (2012). Arl13b in primary cilia regulates the migration and placement of interneurons in the developing cerebral cortex. *Dev. Cell* **23**, 925-938.
Hori, Y., Kobayashi, T., Kikko, Y., Kontani, K. and Katada, T. (2008). Domain architecture of the atypical Arf-family GTPase Arl13b involved in cilia formation. *Biochem. Biophys. Res. Commun.* **373**, 119-124.
Huangfu, D., Liu, A., Rakeman, A. S., Murcia, N. S., Niswander, L. and Anderson, K. V. (2003). Hedgehog signalling in the mouse requires intraflagellar transport proteins. *Nature* **426**, 83-87.
Humbert, M. C., Weihbrecht, K., Searby, C. C., Li, Y., Pope, R. M., Sheffield, V. C. and Seo, S. (2012). ARL13B, PDE6D, and CEP164 form a functional network for INPP5E ciliary targeting. *Proc. Natl. Acad. Sci. USA* **109**, 19691-19696.
Hurd, T. W., Fan, S. and Margolis, B. L. (2011). Localization of retinitis pigmentosa 2 to cilia is regulated by Importin β2. *J. Cell Sci.* **124**, 718-726.
Ishikawa, H., Ide, T., Yagi, T., Jiang, X., Hirono, M., Sasaki, H., Yanagisawa, H., Wemmer, K. A., Stainier, D. Y. R., Qin, H. et al. (2014). TTC26/DYF13 is an intraflagellar transport protein required for transport of motility-related proteins into flagella. *Elife* **3**, e01566.
Ismail, S. A., Chen, Y.-X., Rusinova, A., Chandra, A., Bierbaum, M., Gremer, L., Triola, G., Waldmann, H., Bastiaens, P. I. H. and Wittinghofer, A. (2011). Arl2-GTP and Arl3-GTP regulates a GDI-like transport system for farnesylated cargo. *Nat. Chem. Biol.* **7**, 942-949.
Jonassen, J. A., San Agustin, J., Follit, J. A. and Pazour, G. J. (2008). Deletion of IFT20 in the mouse kidney causes misorientation of the mitotic spindle and cystic kidney disease. *J. Cell Biol.* **183**, 377-384.
Jurczyk, A., Gromley, A., Redick, S., Agustin, J. S., Witman, G., Pazour, G. J., Peters, D. J. M. and Doxsey, S. (2004). Pericentrin forms a complex with intraflagellar transport proteins and polycystin-2 and is required for primary cilia assembly. *J. Cell Biol.* **166**, 637-643.
Katoh, Y., Nozaki, S., Hartanto, D., Miyano, R. and Nakayama, K. (2015). Architectures of multisubunit complexes revealed by a visible immunoprecipitation assay using fluorescent fusion proteins. *J. Cell Sci.* **128**, 2351-2362.
Katoh, Y., Terada, M., Nishijima, Y., Takei, R., Nozaki, S., Hamada, H. and Nakayama, K. (2016). Overall architecture of the intraflagellar transport (IFT)-B complex containing Cluap1/IFT38 as an essential component of the IFT-B peripheral subcomplex. *J. Biol. Chem.* **291**, 10962-10975.
Kimura, Y., Hisano, Y., Kawahara, A. and Higashijima, S. (2014). Efficient generation of knock-in transgenic zebrafish carrying reporter/driver genes by CRISPR/Cas9-mediated genome engineering. *Sci. Rep.* **4**, 6545.
Larkins, C. E., Aviles, G. D. G., East, M. P., Kahn, R. A. and Caspary, T. (2011). Arl13b regulates ciliogenesis and the dynamic localization of Shh signaling proteins. *Mol. Biol. Cell* **22**, 4694-4703.
Li, Y. and Hu, J. (2011). Small GTPases and cilia. *Protein Cell* **2**, 13-25.
Liem, K. F., Jr, Ashe, A., He, M., Satir, P., Moran, J., Beier, D., Wicking, C. and Anderson, K. V. (2012). The IFT-A complex regulates Shh signaling through cilia structure and membrane protein trafficking. *J. Cell Biol.* **197**, 789-800.
Lim, Y. S., Chua, C. E. L. and Tang, B. L. (2011). Rabs and other small GTPases in ciliary transport. *Biol. Cell* **103**, 209-221.
Linari, M., Hanzal-Bayer, M. and Becker, J. (1999). The delta subunit of rod specific cyclic GMP phosphodiesterase, PDE delta, interacts with the Arf-like protein Arl3 in a GTP specific manner. *FEBS Lett.* **458**, 55-59.
Lu, H., Toh, M. T., Narasimhan, V., Thamilselvam, S. K., Choksi, S. P. and Roy, S. (2015). A function for the Joubert syndrome protein Arl13b in ciliary membrane extension and ciliary length regulation. *Dev. Biol.* **397**, 225-236.
Lucker, B. F., Behal, R. H., Qin, H., Siron, L. C., Taggart, W. D., Rosenbaum, J. L. and Cole, D. G. (2005). Characterization of the Intraflagellar Transport Complex B Core: direct interaction of the IFT81 and IFT74/72 subunits. *J. Biol. Chem.* **280**, 27688-27696.
Madhivanan, K. and Aguilar, R. C. (2014). Ciliopathies: the trafficking connection. *Traffic* **15**, 1031-1056.
Mukhopadhyay, S., Wen, X., Chih, B., Nelson, C. D., Lane, W. S., Scales, S. J. and Jackson, P. K. (2010). TULP3 bridges the IFT-A complex and membrane phosphoinositides to promote trafficking of G protein-coupled receptors into primary cilia. *Genes Dev.* **24**, 2180-2193.
Mukhopadhyay, S., Wen, X., Ratti, N., Loktev, A., Rangell, L., Scales, S. J. and Jackson, P. K. (2013). The ciliary G-protein-coupled receptor Gpr161 negatively regulates the Sonic hedgehog pathway via cAMP signaling. *Cell* **152**, 210-223.
Nakatsu, F. (2015). A phosphoinositide code for primary cilia. *Dev. Cell* **34**, 379-380.
Ran, F. A., Hsu, P. D., Wright, J., Agarwala, V., Scott, D. A. and Zhang, F. (2013). Genome engineering using the CRISPR-Cas9 system. *Nat. Protoc.* **8**, 2281-2308.
Romani, M., Micalizzi, A. and Valente, E. M. (2013). Joubert syndrome: congenital cerebellar ataxia with the molar tooth. *Lancet Neurol.* **12**, 894-905.
Schwartz, R. S., Hildebrandt, F., Benzing, T. and Katsanis, N. (2011). Ciliopathies. *N. Engl. J. Med.* **364**, 1533-1543.
Slaats, G. G., Isabella, C. R., Kroes, H. Y., Dempsey, J. C., Gremmels, H., Monroe, G. R., Phelps, I. G., Duran, K. J., Adkins, J., Kumar, S. A. et al. (2016). MKS1 regulates ciliary INPP5E levels in Joubert syndrome. *J. Med. Genet.* **53**, 62-72.
Sung, C.-H. and Leroux, M. R. (2013). The roles of evolutionarily conserved functional modules in cilia-related trafficking. *Nat. Cell Biol.* **15**, 1387-1397.
Swiderski, R. E., Nakano, Y., Mullins, R. F., Seo, S. and Bánfi, B. (2014). A mutation in the mouse *Ttc26* gene leads to impaired hedgehog signaling. *PLOS Genet.* **10**, e1004689.
Takahashi, S., Takei, T., Koga, H., Takatsu, H., Shin, H.-W. and Nakayama, K. (2011). Distinct roles of Rab11 and Arf6 in the regulation of Rab11-FIP3/Arfophilin-1 localization in mitotic cells. *Genes Cells* **16**, 938-950.
Takahashi, S., Kubo, K., Waguri, S., Yabashi, A., Shin, H.-W., Katoh, Y. and Nakayama, K. (2012). Rab11 regulates exocytosis of recycling vesicles at the plasma membrane. *J. Cell Sci.* **125**, 4049-4057.
Taschner, M., Bhogaraju, S. and Lorentzen, E. (2012). Architecture and function of IFT complex proteins in ciliogenesis. *Differentiation* **83**, S12-S22.
Taschner, M., Kotsis, F., Braeuer, P., Kuehn, E. W. and Lorentzen, E. (2014). Crystal structures of IFT70/52 and IFT52/46 provide insight into intraflagellar transport B core complex assembly. *J. Cell Biol.* **207**, 269-282.
Taschner, M., Weber, K., Mourão, A., Vetter, M., Awasthi, M., Stiegler, M., Bhogaraju, S. and Lorentzen, E. (2016). Intraflagellar transport proteins 172, 80, 57, 54, 38, and 20 form a stable tubulin-binding IFT-B2 complex. *EMBO J.* **35**, 773-790.
Thomas, S., Ritter, B., Verbich, D., Sanson, C., Bourbonnière, L., McKinney, R. A. and McPherson, P. S. (2009). Intersectin regulates dendritic spine development and somatodendritic endocytosis but not synaptic vesicle recycling in hippocampal neurons. *J. Biol. Chem.* **284**, 12410-12419.
Van Valkenburgh, H., Shern, J. F., Sharer, J. D., Zhu, X. and Kahn, R. A. (2001). ADP-ribosylation factors (ARFs) and ARF-like 1 (ARL1) have both specific and shared effectors: characterizing ARL1-binding proteins. *J. Biol. Chem.* **276**, 22826-22837.
Warburton-Pitt, S. R. F., Silva, M., Nguyen, K. C. Q., Hall, D. H. and Barr, M. M. (2014). The *nphp-2* and *arl-13* genetic modules interact to regulate ciliogenesis and ciliary microtubule patterning in *C. elegans*. *PLOS Genet.* **10**, e1004866.
Wei, Q., Ling, K. and Hu, J. (2015). The essential roles of transition fibers in the context of cilia. *Curr. Opin. Cell Biol.* **35**, 98-105.

Supplementary materials

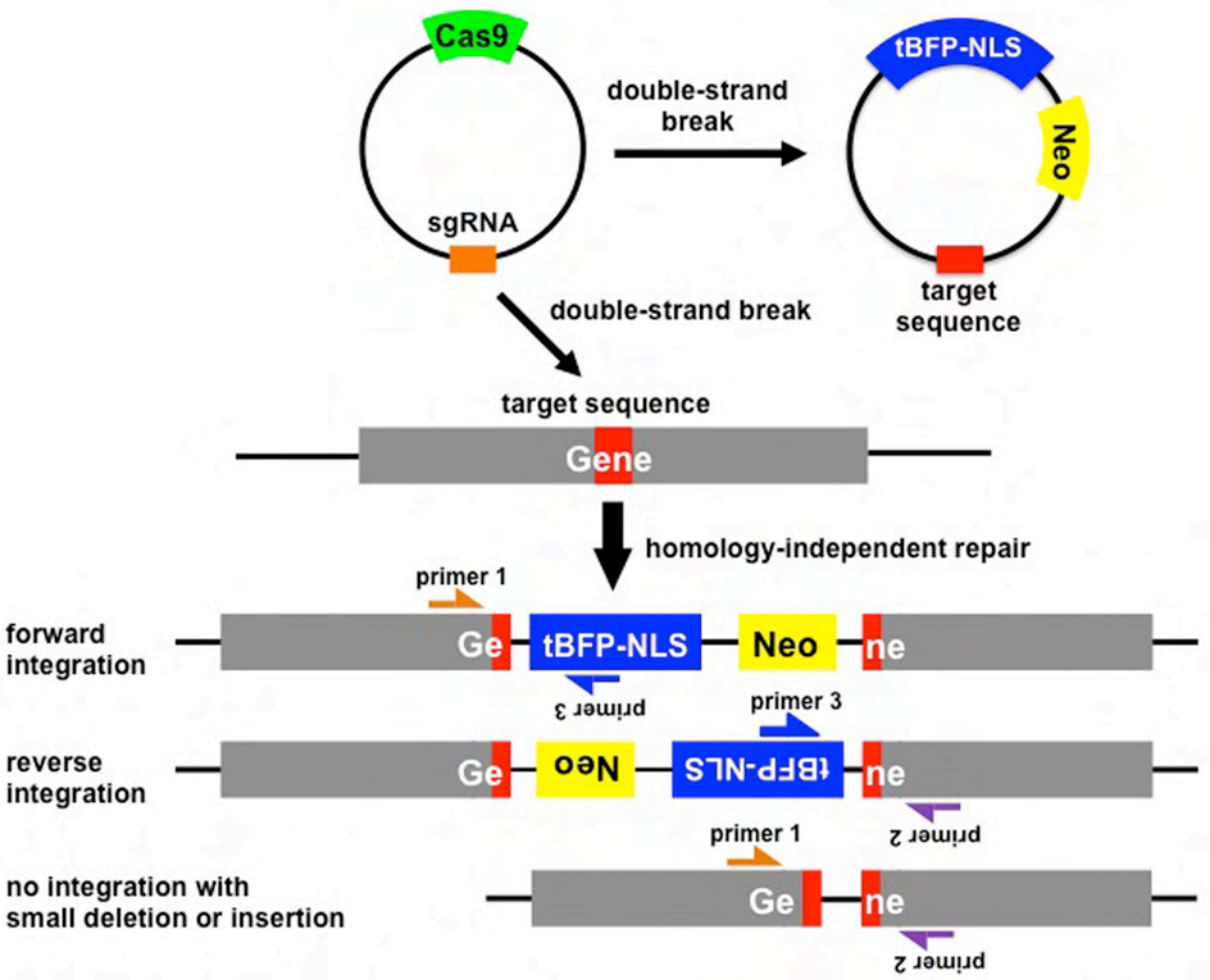

Fig. S1. Strategy for establishment of hTERT-RPE1 KO cell lines using a modified CRISPR/Cas9 system

An expression vector for Cas9 (light green) containing sgRNA sequence (orange) and a donor knock-in vector containing a tBFP-3×NLS sequence (blue) and the Neo gene (yellow) for clonal selection are co-transfected into hTERT-RPE1 cells. Cas9 generates DNA double-strand breaks at the target sequences (red) in the donor knock-in vector and in the target gene, thereby inducing homology-independent DNA repair. Upon repair, two types of donor vector integration can occur; forward integration and reverse integration. In addition, the target gene can often be repaired incompletely with a small deletion or insertion, causing a frameshift. After selection of the transfected clones by culturing cells in the presence of G418 and the detection of nuclear BFP signals, genomic DNA was extracted from the selected cells and subjected to PCR using primer pairs that can distinguish between alleles with forward integration (pair b: primers 1 + 3) or reverse integration (pair c: primers 2 + 3) of the donor knock-in vector, or alleles with a small deletion, insertion, or no repair (pair a: primers 1 + 2). Half-headed arrows represent primers used for genomic PCR.

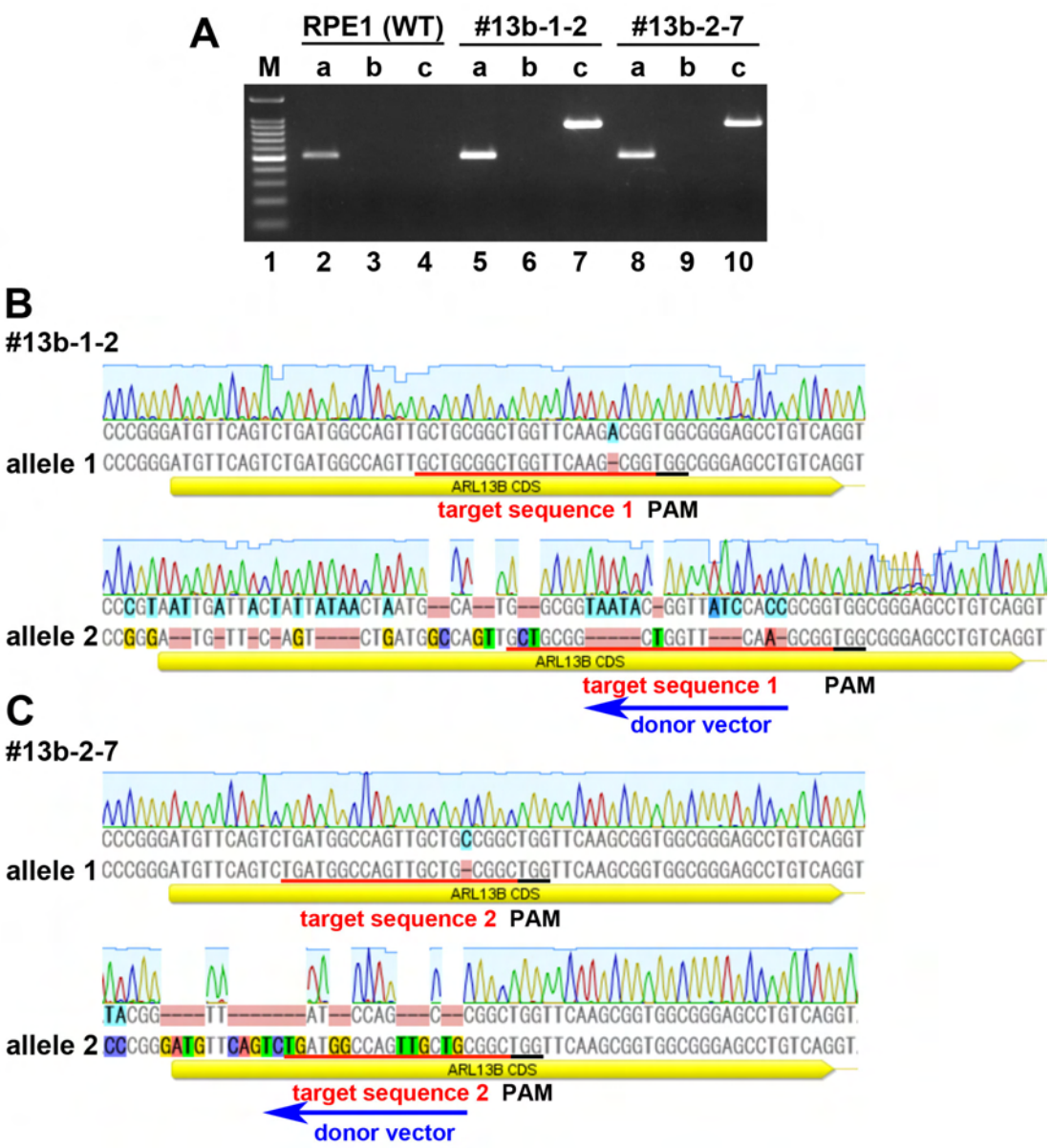

Fig. S2. Genomic PCR and sequencing to confirm donor vector integration or small deletions or insertions in the selected *ARL13B*-KO cell lines

(A) Genomic DNA was extracted from control hTERT-RPE1 cells (lanes 2–4), and from *ARL13B*-KO cell lines (#13b-1-2, lanes 5–7; and #13b-2-7, lanes 8–10) established using a donor knock-in vector containing target sequences 1 and 2, respectively (see Table S2), both of which target the coding region within exon 1 of the human *ARL13B* gene. The DNA was subjected to PCR using the primer pair a (primers 1 + 2; lanes 2, 5, and 8), pair b (primers 1 + 3; lanes 3, 6, and 9), or pair c (primers 2 + 3; lanes 4, 7, and 10) (see Table S3) to detect alleles with a small insertion, deletion, or no repair, with donor vector forward integration, and reverse integration, respectively. Lane 1, a 100-bp ladder marker in which the most intense band is 500 bp. (B) and (C), alignments of allele sequences of cell lines #13b-1-2 and #13b-2-7 determined by direct sequencing of the genomic PCR products with the reference sequence encompassing the coding sequence of exon 1. Red and black lines indicate the target sequences and PAM sequence, respectively. Blue arrows indicate the direction of vector integration.

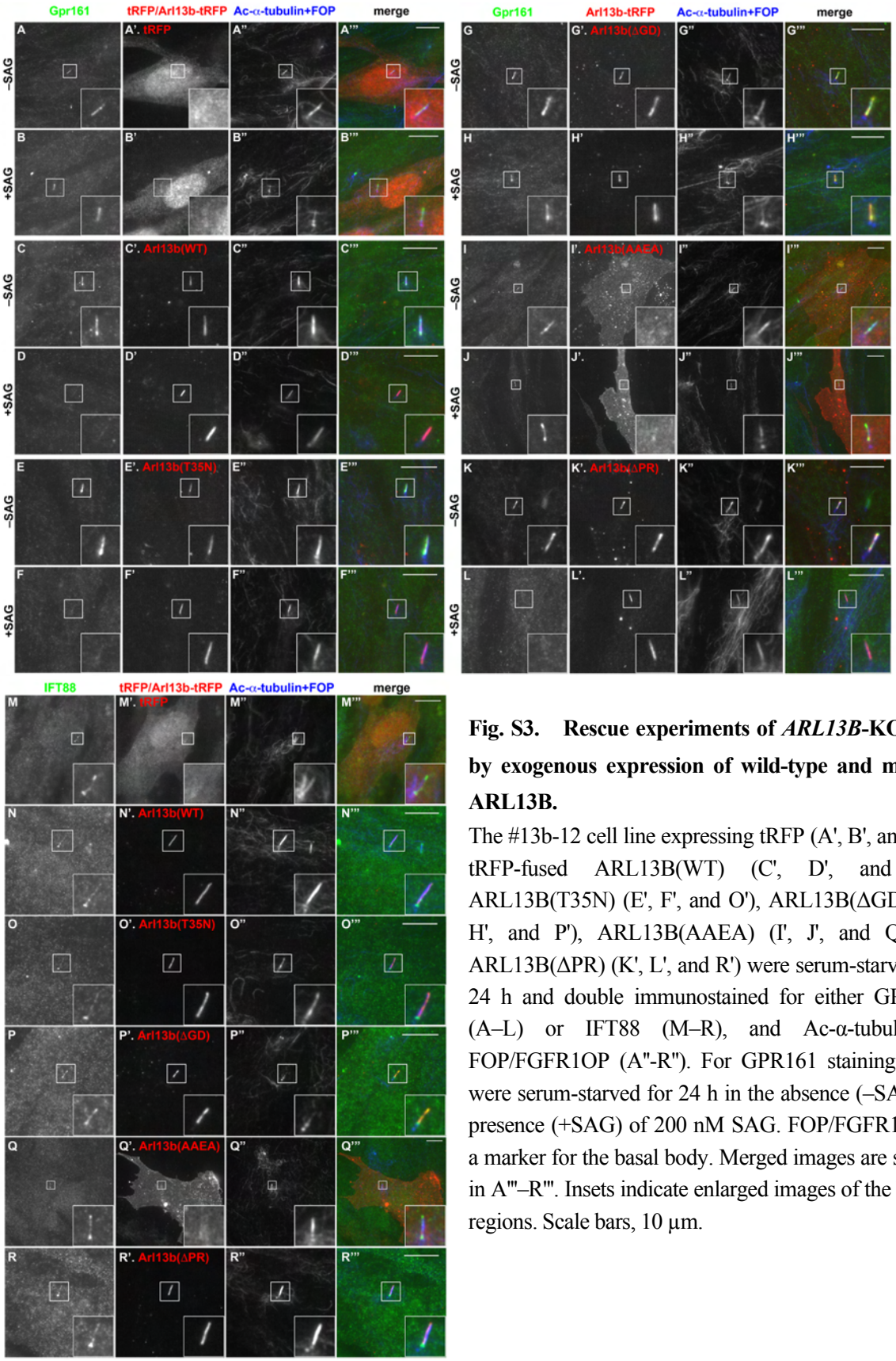

Fig. S3. Rescue experiments of *ARL13B*-KO cells by exogenous expression of wild-type and mutant ARL13B.

The #13b-12 cell line expressing tRFP (A', B', and M'), tRFP-fused ARL13B(WT) (C', D', and N'), ARL13B(T35N) (E', F', and O'), ARL13B(ΔGD) (G', H', and P'), ARL13B(AAEA) (I', J', and Q'), or ARL13B(ΔPR) (K', L', and R') were serum-starved for 24 h and double immunostained for either GPR161 (A–L) or IFT88 (M–R), and Ac-α-tubulin + FOP/FGFR1OP (A"-R"). For GPR161 staining, cells were serum-starved for 24 h in the absence (–SAG) or presence (+SAG) of 200 nM SAG. FOP/FGFR1OP is a marker for the basal body. Merged images are shown in A'"–R'". Insets indicate enlarged images of the boxed regions. Scale bars, 10 µm.

Table S1. Plasmid vectors used in this study

No.	Vectors	Inserts
1	pCAG-dS-EGFP-N	ARL13B
2	pCAG-dS-EGFP-N	ARL13B(T35N)
3	pCAG-dS-EGFP-N	ARL13B(R79Q)
4	pCAG-dS-EGFP-N	ARL13B(ΔGD; 1-19, 190-428 aa)
5	pCAG-dS-EGFP-N	ARL13B(Arf6GD; 1-19, 190-428 aa_ARL13B; 5-172 aa_ARF6)
6	pCAG-dS-EGFP-N	ARL13B(R200C)
7	pCAG-dS-EGFP-N	ARL13B(ΔCC; 1-189, 245-428 aa)
8	pCAG-dS-EGFP-N	ARL13B(AAEA; RVEP358-361AAEA)
9	pCAG-dS-EGFP-N	ARL13B(ΔPR; 1-361 aa)
10	pCAG-dS-tRFP-N	ARL13B
11	pCAG2-mCherry-N	ARL13B
12	pCAG2-mCherry-N	ARL13B(T35N)
13	pCAG2-mCherry-N	ARL13B(R79Q)
14	pCAG2-mCherry-N	ARL13B(ΔGD; 1-19, 190-428 aa)
15	pCAG2-mCherry-N	ARL13B(Arf6GD; 1-19, 190-428 aa_ARL13B; 5-172 aa_ARF6)
16	pCAG2-mCherry-N	ARL13B(R200C)
17	pCAG2-mCherry-N	ARL13B(ΔCC; 1-189, 245-428 aa)
18	pCAG2-mCherry-N	ARL13B(AAEA; RVEP358-361AAEA)
19	pCAG2-mCherry-N	ARL13B(ΔPR; 1-361 aa)
20	pRRLsinPPT-TagRFP-T-N	ARL13B
21	pRRLsinPPT-TagRFP-T-N	ARL13B(T35N)
22	pRRLsinPPT-TagRFP-T-N	ARL13B(R79Q)
23	pRRLsinPPT-TagRFP-T-N	ARL13B(ΔGD; 1-19, 190-428aa)
24	pRRLsinPPT-TagRFP-T-N	ARL13B(Arf6GD; 1-19, 190-428 aa_ARL13B; 5-172 aa_ARF6)
25	pRRLsinPPT-TagRFP-T-N	ARL13B(R200C)
26	pRRLsinPPT-TagRFP-T-N	ARL13B(ΔCC; 1-189,245-428aa)
27	pRRLsinPPT-TagRFP-T-N	ARL13B(AAEA; RVEP358-361AAEA)
28	pRRLsinPPT-TagRFP-T-N	ARL13B(ΔPR; 1-361 aa)
29	pCAG-mCherry-C	INPP5E
30	pRRLsinPPT-EGFP-C	TULP3
31	pEBMulti-Ble-EGFP	2xP4M^{SidM} (Addgene plasmid #51472)
32	pEGFP-N1	mouse PLCδ-PH (1-170)
33	pTagRFP-T-N	IFT20
34	pTagRFP-T-C	IFT22
35	pTagRFP-T-C	IFT25
36	pTagRFP-T-C	IFT27
37	pTagRFP-T-C	IFT38
38	pCAG-mCherry-C	IFT46
39	pCAG-mCherry-C	IFT52
40	pTagRFP-T-C	IFT54
41	pCAG2-tRFP-T-C	IFT56

42	pTagRFP-T-C	IFT57
43	pCAG-mCherry-C	IFT70
44	pCAG-mCherry-C	IFT74
45	pCAG-mCherry-N	IFT80
46	pCAG-mCherry-C	IFT81
47	pCAG-mCherry-C	IFT88
48	pCAG-mCherry-C	IFT172
49	pCAG-EGFP-C	IFT46
50	pCAG2-EGFP-C	IFT56
51	pGEX-6P1	GFP-Nb

Table S2. Antibodies used in this study

Antibodies	Manufacturers	Clone or catalog numbers	Dilution (purpose)
Monoclonal mouse anti-Ac-α-tubulin	Sigma-Aldrich	6-11B-1	1:500 (immunofluorescence)
Monoclonal mouse anti-γ-tubulin	Sigma-Aldrich	GTU88	1:1,000 (immunofluorescence)
Polyclonal rabbit anti-ARL13B	Proteintech	17711-1-AP	1:1,000 (immunofluorescence)
Polyclonal rabbit anti-IFT88	Proteintech	13967-1-AP	1:200 (immunofluorescence)
Polyclonal rabbit anti-IFT140	Proteintech	17460-1-AP	1:100 (immunofluorescence)
Polyclonal rabbit anti-INPP5E	Proteintech	17797-1-AP	1:500 (immunofluorescence)
Polyclonal rabbit anti-GPR161	Proteintech	13398-1-AP	1:200 (immunofluorescence)
Polyclonal rabbit anti-SMO	Abcam	ab38686	1:100 (immunofluorescence)
Monoclonal mouse anti-FOP	Abnova	2B1	1:10,000 (immunofluorescence)
Monoclonal mouse anti-GFP	BD Biosciences	JL-8	1:1,000 (immunoblotting)
Polyclonal rabbit anti-RFP	MBL Life Science	PM005	1:1,000 (immunoblotting)
Polyclonal rabbit anti-tRFP	Evrogen	AB233	1:1,000 (immunoblotting)
AlexaFluor-conjugated secondary	Molecular Probes	A21240, A11034, A21127	1:1,000 (immunofluorescence)
DyLight 649-conjugated secondary	Jackson ImmunoResearch	115-495-209	1:1,000 (immunofluorescence)
Peroxidase-conjugated secondary	Jackson ImmunoResearch	115-035-166, 111-035-144	1:3,000 (immunoblotting)

Table S3. Oligo DNAs used in this study

No.	Names	Sequences
1	ARL13B-genome-FW	5'-GCTAACTCGGCTACGGTGTATC-3'
2	ARL13B-genome-RV	5'-CAACGGTAAGCATTGTCAATCGC-3'
3	pTagBFP-N-RV	5'-GTTGTCCACGGTGCCCTCCATGTAC-3'
4	ARL13B-gRNA#1-S	5'-CACCGCTGCGGCTGGTTCAAGCGG-3'
5	ARL13B-gRNA#1-AS	5'-AAACCCGCTTGAACCAGCCGCAGC-3'
6	ARL13B-Donor#1-AS	5'-TCCACCGCTTGAACCAGCCGCAGC-3'
7	ARL13B-gRNA#2-S	5'-CACCGTGATGGCCAGTTGCTGCGGC-3'
8	ARL13B-gRNA#2-AS	5'-AAACGCCGCAGCAACTGGCCATCAC-3'
9	ARL13B-Donor#2-AS	5'-TCCAGCCGCAGCAACTGGCCATCAC-3'